BNL-212469-2019-TECH

EIC/69

Cryogenic RF tests of US LARP DQW SPS-series cavities

S. Verdu-Andres

October 2019

Collider Accelerator Department

Brookhaven National Laboratory

U.S. Department of Energy

USDOE Office of Science (SC), Nuclear Physics (NP) (SC-26)

Notice: This technical note has been authored by employees of Brookhaven Science Associates, LLC under Contract No.DE-SC0012704 with the U.S. Department of Energy. The publisher by accepting the technical note for publication acknowledges that the United States Government retains a non-exclusive, paid-up, irrevocable, world-wide license to publish or reproduce the published form of this technical note, or allow others to do so, for United States Government purposes.

DISCLAIMER

This report was prepared as an account of work sponsored by an agency of the United States Government. Neither the United States Government nor any agency thereof, nor any of their employees, nor any of their contractors, subcontractors, or their employees, makes any warranty, express or implied, or assumes any legal liability or responsibility for the accuracy, completeness, or any third party's use or the results of such use of any information, apparatus, product, or process disclosed, or represents that its use would not infringe privately owned rights. Reference herein to any specific commercial product, process, or service by trade name, trademark, manufacturer, or otherwise, does not necessarily constitute or imply its endorsement, recommendation, or favoring by the United States Government or any agency thereof or its contractors or subcontractors. The views and opinions of authors expressed herein do not necessarily state or reflect those of the United States Government or any agency thereof.

Cryogenic RF tests of US LARP DQW SPS-series cavities*

Silvia Verdú-Andrés† and Ilan Ben-Zvi[1], Binping Xiao, Qiong Wu
BNL, NY 11973, Upton, USA

Rama Calaga and Ofelia Capatina
CERN, Geneva 23, CH 1211, Switzerland

Naeem Huque, Anne McEwen, HyeKyoung Park, Tom Powers and Haipeng Wang
JLAB, Newport News, VA 23606, USA

Graeme Burt[2] and James Alexander Mitchell
Lancaster University, Bailrigg, LA1 4YW, UK

Zenghai Li and Alex Ratti
SLAC, Menlo Park, CA 94025, USA
(Dated: October 24, 2019)

Crab cavities are one of the several components included in the luminosity upgrade of the Large Hadron Collider (HL-LHC). For nominal operation, the cavities have to provide a nominal deflecting kick of 3.4 MV per cavity in Continuous Wave operation at 2 K. The requirement for an unjacketed cavity – bare cavity equipped with Higher-Order Mode (HOM) filters and field antenna – is to reach at least a deflecting voltage of 4.1 MV (20% margin) with the heat load to the 2 K bath below 10 W. Cryogenic RF tests confirmed the required performances in bare cavities, with several cavities exceeding the required voltage by more than 50%. However, the first tests of a Double-Quarter Wave (DQW) cavity with one out of three HOM filters did not reach the required voltage. The present paper describes the studies and tests conducted to understand the limiting factor in the operation of a DQW cavity with HOM filters in the most up-to-date prototypes produced in the US and based on the DQW SPS-series design. The recipe to meet the performance specification for a bare DQW cavity with HOM filters and exceed the voltage requirement by more than 35% is discussed.

CERN EDMS No. 2258403: `https://edms.cern.ch/document/2258403`

* Work supported by the US DOE through the US LHC Accelerator Research Program (LARP) and through Brookhaven Science Associates LLC under contract No. DE-SC0012704. Also supported by the European Union HL-LHC Project.
† Corresponding author: `sverdu@bnl.gov`

CONTENTS

I. INTRODUCTION

Crab cavities are one of the several components included in the baseline luminosity upgrade of the Large Hadron Collider (HL-LHC) [1]. The HL-LHC crab cavities need to deliver a nominal deflecting kick of 3.4 MV per cavity at 400 MHz in Continuous Wave (CW) operation mode at 2 K. In cold tests of unjacketed cavities, the cavities should reach at least a deflecting voltage of 4.1 MV (20% margin). This margin is intended to cover for possible voltage degradation observed in other SRF cavities after jacketing. The heat load per dressed (unjacketed) cavity – cavity with HOM filters and field pickup – shall not exceed 10 W at 4.1 MV. The operation requirements for the HL-LHC crab cavities are summarized in Table I [2].

Crabbing frequency	400.79	MHz
Nominal deflecting voltage ($V_{t,nom}$)	3.4	MV
Target deflecting voltage for unjacketed cavity ($V_{t,unj}$)	4.1	MV
Heat load at $V_{t,unj}$	10	W

TABLE I: Operational requirements for a HL-LHC crab cavity

An array of Double-Quarter Wave (DQW) cavities will provide the vertical deflecting kick for crab crossing in HL-LHC [3]. The DQW cavities are compact, superconducting RF cavities which fundamental mode provides a transverse deflecting kick [4]. In LHC, the second beam pipe imposes a tight spacial constraint to the cavity's width. The HL-LHC DQW cavities have a "waist" to accommodate the second beam pipe and the cavity's height is chosen to meet the tight spacial constraint, so the cavities can be used for crab crossing in both the vertical and horizontal planes [5, 6] as illustrated in Fig. 1. All the HL-LHC DQW cavities present an elliptical cross section that enhances the figure of merit of maximum peak surface magnetic field over deflecting voltage (B_p/V_t).

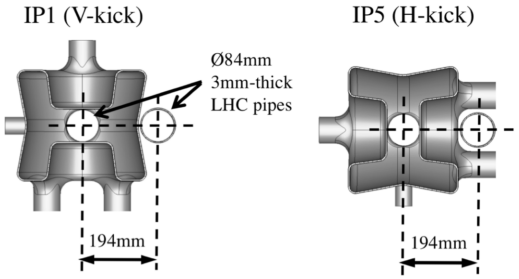

FIG. 1: The DQW cavity satisfies the LHC geometric constraints imposed by the second beam pipe to provide a deflecting kick for both vertical and horizontal crossing planes.

This report is organized as follows. Firstly, a brief description of the HL-LHC DQW design evolution is provided describing the different prototypes available, their similarities and differences. The design evolution of the Higher-Order Mode (HOM) filters is discussed elsewhere [7–10]. Then, the cryogenic RF test campaign to validate the operation of a DQW SPS-series cavity at nominal deflecting voltage and search for its ultimate performances is discussed.

A. The DQW PoP-Series

A first DQW cavity was designed and fabricated in 2012 to validate the DQW concept. The Proof-of-Principle (DQW PoP-series) cavity has 6 dummy ports. These dummy ports, with a diameter of only 20 mm, are not intended to handle the large power levels required for adequate fundamental power coupling and HOM power extraction during operation with beam, but to ensure cleaning of the high-magnetic field region and host the test probes. The largest peak magnetic field is found in the blending of the dummy ports (B_p/V_t = 25.1 mT/MV). The DQW PoP-series cavity is shown in Fig. 2. Table II lists the RF properties of the PoP-series DQW cavity.

The cryogenic RF tests of a DQW PoP-series prototype in 2014 demonstrated reliable operation beyond the 3.4 MV required for HL-LHC, reaching 116 mT before quench at 4.6 MV [5].

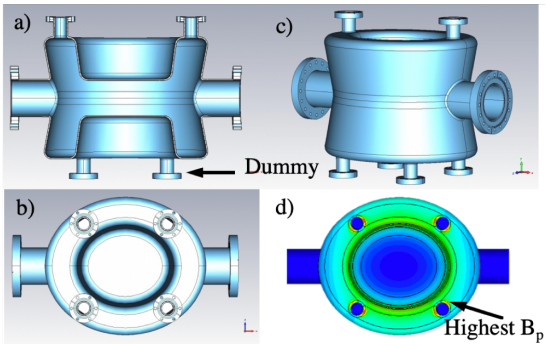

FIG. 2: The DQW PoP-series cavity: a) cross-section side view; b) bottom; c) perspective view; d) magnetic field distribution using 5-color heatmap scale.

B. The DQW SPS-Series

The validation of the DQW concept with the PoP-series prototype was the first step towards the preparation of a fully-equipped DQW cryomodule for beam tests in the Super Proton Synchrotron (SPS) of CERN. The two cavities inside of the cryomodule were based on the DQW SPS-series design, an evolution of the PoP-series compliant with the LHC requirements for fundamental and HOM power handling, heat load, tunability, shielding, and stiffening, all perfectly integrated into its own cryomodule. The DQW cavity design was revisited to incorporate larger, 62 mm-diameter ports to supply the required fundamental mode power and sufficiently damp the HOM power induced by the LHC beam during operation [6, 11]. A DQW SPS-series cavity has 4 large ports, one for the Fundamental Power Coupler (FPC) and three for the HOM filters. Fig. 3 depicts the nominal setup for a dressed DQW SPS-series cavity.

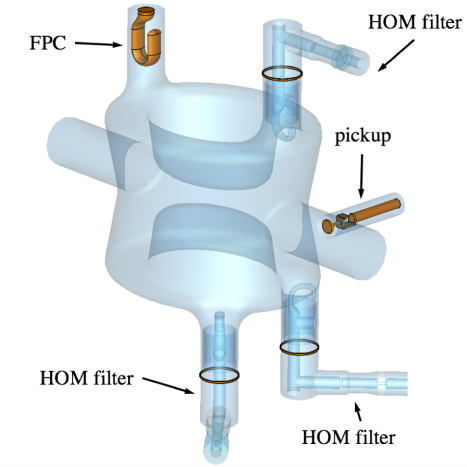

FIG. 3: Dressed DQW SPS-series cavity.

All 3 HOM filters of a DQW SPS-series cavity are identical and specifically designed to damp sufficiently the HOM power from the LHC beam [7]. The S21 parameter for the HOM filters is shown in Fig. 4. The DQW HOM filter provides a deep, broad notch (at least -80 dB deep and broader than 10 MHz) centered around the fundamental mode frequency at 400 MHz. The deep, broad notch ensures a good rejection of fundamental mode power through the HOM filter port. The filter response changes quickly for frequencies above the fundamental mode, showing good transmission for frequencies above the first HOM of the DQW cavity at 570 MHz. Only one mode, at 1.754 GHz, is insufficiently coupled through the HOM port apertures. The power of this mode is extracted through a small port opened in one of the beam pipes. This small port hosts a dual-function antenna. The hook section couples to the fundamental mode to extract sufficient power for monitoring of the cavity's field and control purposes. The T-section couples electrically to the 1.754 GHz mode [12].

The new cavity-port interface is optimized to reduce the B_p/V_t with respect to the PoP-series, so the maximum peak surface magnetic field is 11% lower. The highest field is located in the cavity body, in between the two HOM ports, not in the filter. Fig. 5 displays the magnetic field distribution in the cavity and HOM filter. To enable a smooth interface, the elliptical racetrack of the PoP-series is modified for the SPS-series to have a constant width. The DQW SPS-series design also satisfies

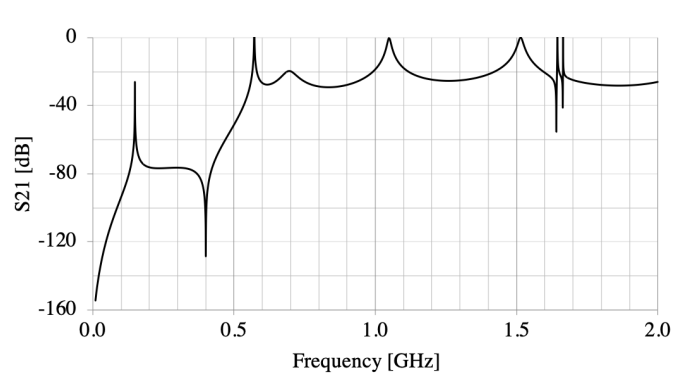

FIG. 4: S21 parameter for the HOM filter of DQW SPS-series cavity.

the spatial constraints imposed by the second beam pipe of LHC to provide crabbing kick in both vertical and horizontal configurations. Table II lists the RF properties of the DQW SPS-series cavity.

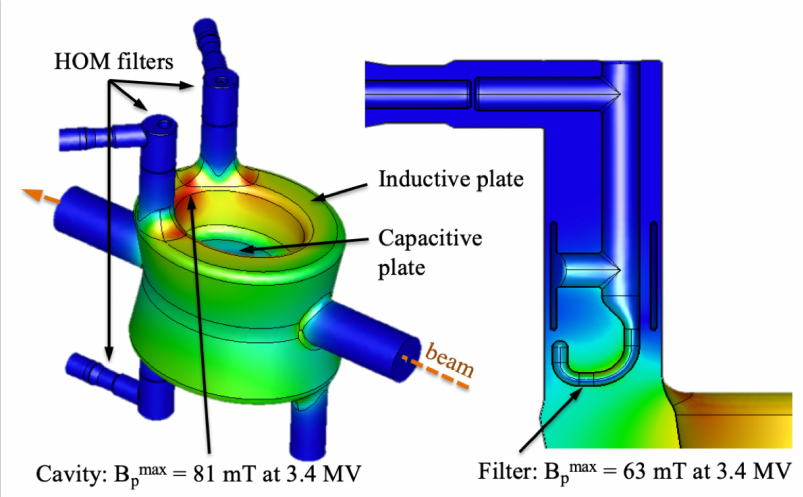

FIG. 5: Magnetic field distribution of the fundamental mode using 5-color heatmap scale for: [left] cavity and [right] section view of HOM filter.

Four identical cavities were fabricated based on the DQW SPS-series design [13]: two prototypes built under the umbrella of the US LHC Accelerator Research Program (LARP) by Niowave Inc. and JLab [6] and two other built, fully dressed, and assembled into a cryomodule by CERN for beam tests in the Super Proton Synchrotron (SPS) [14]. Eight HOM filters were fabricated by CERN[15].

The following sections will summarize the test campaign undertaken by the collaboration to validate the operation at nominal deflecting voltage of the DQW SPS-series design and evaluate its ultimate performance. The reader will note that the first test involving the bare cavity DQW01 led to remarkable high fields (125 mT, 65 MV/m) and deflecting voltage (5.9 MV). Later tests of cavity plus HOM filter found its performance limited to barely the nominal deflecting voltage. Simulation and experimental efforts to identify the source of this diminished performance will be explained and the solution to improve the performance will be presented.

Series	**PoP** [5]	**SPS** [6, 7, 16]	**LHC** [11]	
Scope	Validation of DQW concept; only bare cavity, no HOM filters	Design fully adequate for beam operation (input power, HOM damping, tuning, integration); evaluation with beam in SPS	Operation in LHC	
Cavity design	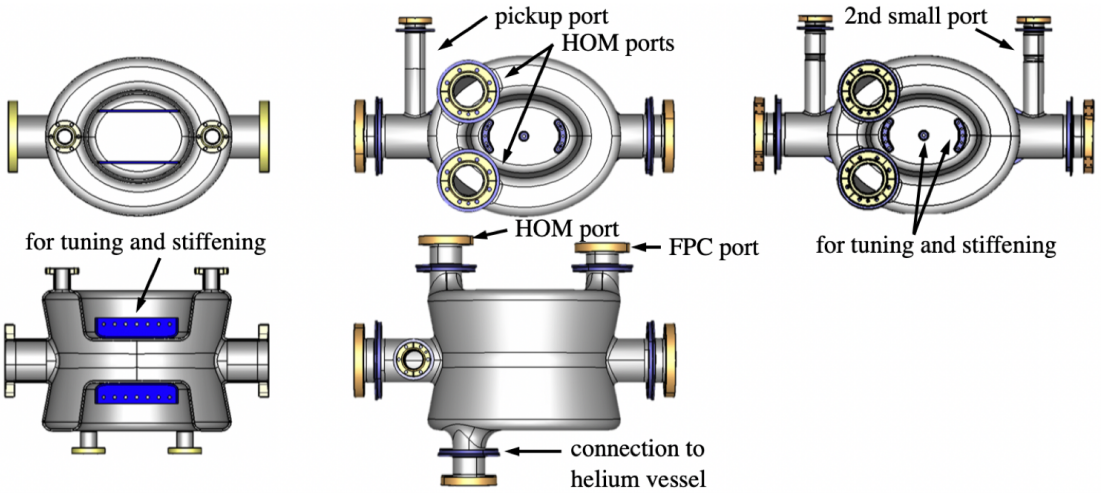			
Design evolution	*From PoP to SPS*: 1) Update port size for adequate coupling to fundamental and HOM damping; 2) Optimize port blend to lower Bp (involved changing racetrack profile); and 3) Design compatible with cryomodule, incl. tuner, stiffening, shielding for adequate heat load. *From SPS to LHC*: 1) Second small port to host dedicated 1.754 GHz antenna; and 2) Extend short beam pipe to reduce loss in joint.			
Electromagnetic properties				
RF frequency (crabbing, fundamental mode)	400	400	400	MHz
Max. Bp at nominal Vt (cavity / filter)	85.4 /–	72.8/ 56.6	72.8 /–	mT
Max. Ep at nominal Vt (cavity / filter)	36.5 / –	37.7/ 29.0	37.7/ –	MV/m
Geometric shunt impedance (Rt/Q)	406	429	429	Ω
Geometry factor (G)	85	87	87	Ω
Manufactured cavities				
US LARP	1	2	–	
Manufacturer	Niowave	Niowave + JLab	–	
VT facility	BNL	JLab	–	
HL-LHC WP4	–	2 (in DQW cryomodule)	–	
Manufacturer	–	CERN	–	
VT facility	CERN	CERN	–	
VT results	Exceeds nominal V_t with 38% margin	Exceeds nominal V_t with 38% margin (up to 73% w/o HOM filters); heat load below 5 W as required (R_s = 9 nΩ); FE onset above nominal V_t	Similar performance than SPS-series expected: changes only impact the cavity ports and antennae, not the cavity body where peak fields are located	

TABLE II: Comparison between different design series of the HL-LHC DQW cavity

II. MATERIALS & METHODS

All the vertical tests discussed in Section III were performed at the SRF test facility of JLab. All the cavities were based on the DQW SPS-series design and manufactured by Niowave Inc. and JLab in the framework of LARP; the HOM filters were manufactured by CERN. Data displayed below, unless otherwise indicated, was taken when the cavities were fully immersed in a superfluid helium bath at 2.0 K. The tests evaluated the performance of unjacketed: bare and dressed cavities.

A. Port configuration, dissipative losses

The DQW SPS-series cavity has four DN63 ports opened on the inductive region and two DN100 ports to allow for the passage of the beam. One DN40 port is opened on one of the beam ports for extraction of HOM power and sampling of the fundamental mode signal. Fig. 6 shows the ports of the cavity. The position of each port connection with respect to the cavity center is listed in Table III.

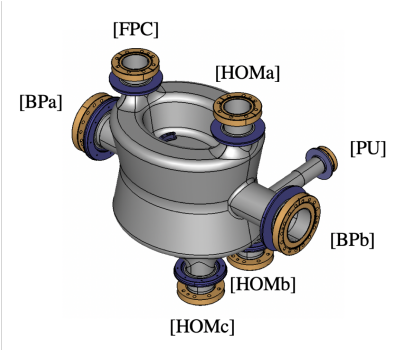

FIG. 6: Ports of the DQW SPS-series cavity.

TABLE III: Distance of port connection to cavity center at room temperature

Port	Direction	Position (mm)
FPC	y	240.3
HOMa	y	255.4
HOMb	y	255.4
HOMc	y	255.4
BPa	z	309.8
BPb	z	349.8
PU	x	245.7

A DQW SPS-series cavity is made of RRR>300 niobium. Flanges are made of non-magnetic stainless steel grade 316LN. Gaskets are made from OFE/OHCO copper. RF-seal gaskets are used in some port connections to reduce the exposure of stainless steel to the RF field. Some of the blank flanges are coated with a thin (100 µm-thick) film of niobium to reduce their heat load. Table IV contains the RF surface resistance value used to evaluate the dissipative losses of each component [17]. The value for copper considers the anomalous skin effect of copper at 2 K and 400 MHz with a 30% corrective factor to account for the increase in RF surface resistance due to the surface roughness [18].

Material	$R_S(\Omega)$
Copper	1×10^{-3}
Stainless steel	3×10^{-2}
Niobium	20×10^{-9}

TABLE IV: RF surface resistance (R_s) values used to evaluate the dissipative losses of the different components in a DQW SPS-series cavity during a 2 K cryogenic RF test

The test probes used during cold tests of the DQW SPS-series cavities, their location and orientation are shown in Fig. 7. The external coupling factor Q_e for each test probe is listed in Table V [19]. Table VI lists the intrinsic quality factor for each component assuming the RF surface resistance values provided in Table IV. This table also contains the power dissipated in each component for operation at nominal deflecting voltage (3.4 MV). Table VII collects the contribution of each HOM filter when assembled to the bare cavity. Most of the power is dissipated in the input probe and its feedthrough. Still, the expected quality factor of the cavity (1×10^{10} for R_s of 9 nΩ) is one order of magnitude smaller than the total quality factor of the rest of components (3.17×10^{11}). That is, for a bare cavity at nominal deflecting voltage, the cavity walls would dissipate 2.71 W while the rest of components would only dissipate 0.09 W (here we assume that the quality factor of the cavity does not degrade at high fields). Some assumptions were made when computing the contributions of each component:

- The calculations consider that the input probe temperature stays constant at 2 K. In reality, the probe might be at higher temperature during operation, implying larger dissipative losses due to increased surface resistance.
- Flanges are thermally intercepted at 2 K and there is ideal heat conduction from flanges to RF-seal gaskets, so the RF-seal gaskets will also be 2K despite being exposed to the electromagnetic field.

- Only the fundamental (operating) mode contributes significantly to the heat load.
- The surface of the flange hole has not been coated, so this surface is stainless steel.

Test probe	Q_e
Input	2.3×10^{9}
Pickup	8.0×10^{11}

TABLE V: External quality factor for designed test probes

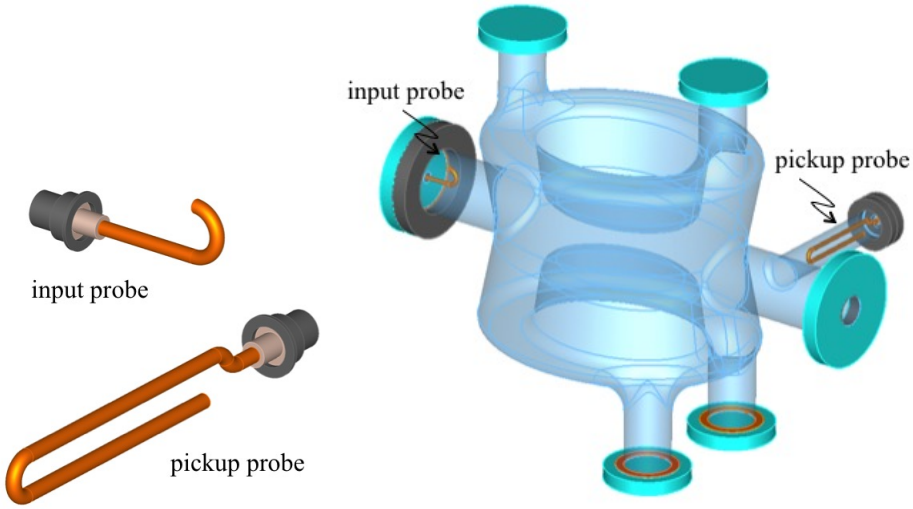

FIG. 7: [Left] Test probes for DQW SPS-series cavity cold tests. [Right] Location and orientation of the test probes, valid for both bare and dressed cavity cold tests.

B. Instrumentation

The cavity temperature was monitored by an array of eight CERNOX thermosensors. The location of the thermosensors varied from test to test. When discussing the results of a test, a number between 1 and 8 will be provided for each thermosensor (corresponding to the channel number in the scope display) together with the letter denoting its location during that particular test. Fig. 8 illustrates the possible locations for the thermosensors. These locations were:

- #A: Highest magnetic field region in the whole assembly (including HOM filters).
- #B: On top of blank-off, Nb-coated flange of the shortest 62-mm port, the FPC port.
- #C: On top of blank-off, Nb-coated flange. First point in the cavity to experience a temperature drop if the helium level is insufficient to fully cover the cavity.
- #D: On top of the HOM01 filter, next to the cooling channel. Note that the cap of the HOM01 helium jacket is missing to allow the installation of a thermosensor around the cooling channel during these cold tests.
- #E: Redundancy of #D.
- #F: On the inner conductor blending at the base of the HOM01 port. The highest magnetic field region for this port.
- #G: Inside of the helium jacket of HOM02 filter. Note that the helium jacket of the HOM02 jacket is fully assembled, so the only way to monitor the temperature near the cooling channel of the HOM filter is to insert the thermosorts through the inlet of the helium jacket.
- #H: Redundancy of #F.

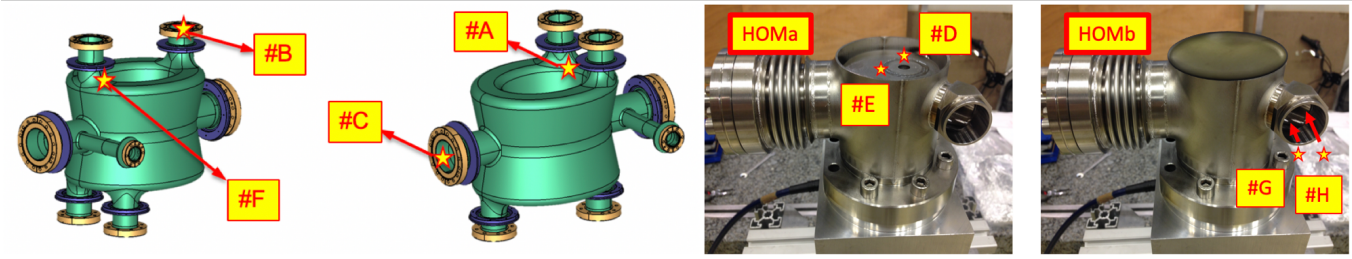

FIG. 8: Thermosensor map.

C. Stiffening frame

The cavities were mounted on one of the JLab standard stiffening frames. The frame was adapted to fix the two capacitive plates of the DQW cavity in three points: one at the center of each plate and two other rods fixing the side of each plate. Fig 9 shows the DQW cavity assembled into the stiffening frame. The central rods were not used for tests conducted in 2018 and 2019 because the thread on the stiffening rod adapter welded to the cavity was damaged.

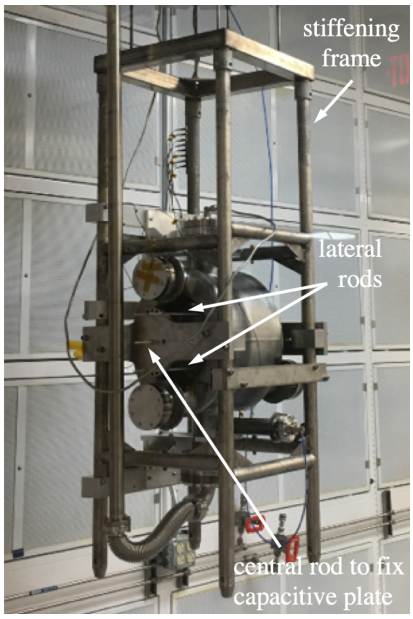

FIG. 9: Stiffening frame used for cryogenic RF tests of DQW cavities in JLab. The central rods were removed for tests conducted in 2018 and 2019.

Port	Status	Component	Surface material	Q_0	$P_{0,nom}$(W)
FPC	Blanked	Flange	Niobium film	2.36e16	1.14e-6
		RF-seal gasket	Copper	6.89e12	3.91e-3
HOMa	Blanked	Flange	Niobium film	1.42e17	1.90e-7
		RF-seal gasket	Copper	4.16e13	6.47e-4
HOMb	Blanked	Flange	Niobium film	1.18e17	2.29e-7
		RF-seal gasket	Copper	3.44e13	7.83e-4
HOMc	Blanked	Flange	Niobium film	1.17e17	2.29e-7
		RF-seal gasket	Copper	3.44e13	7.82e-4
BPa	Test input	Flange	Niobium film	1.18e17	2.28e-7
		Feedthru	Stainless steel	2.29e12	1.18e-2
		RF-seal gasket	Copper	4.68e13	5.76e-4
		Input probe	Copper	4.17e11	6.46e-2
BPb	Vacuum	Flange	Niobium film	4.46e18	6.03e-9
		Flange hole	Stainless steel	1.46e13	1.84e-3
		RF-seal gasket	Copper	1.32e15	2.05e-5
PU	Test pickup	Flange and feedthru	Stainless steel	1.23e15	2.18e-5
		Conventional gasket	Copper	1.16e18	2.33e-8
		Pickup probe	Copper	1.56e15	1.73e-5
TOTAL				3.17e11	8.50e-2

TABLE VI: Bare cavity cold test port configuration. Intrinsic quality factor Q_0 per component and associated power loss P_0 at nominal deflecting voltage $V_{t,nom}$ (3.4 MV)

Port	Status	Component	Surface material	Q_0	$P_{0,nom}$(W)
HOMa	HOM filter	Filter	Niobium		3e-2
		RF-seal gasket	Copper	3.45e12	7.8e-3
HOMb	HOM filter	Filter	Niobium		3e-2
		RF-seal gasket	Copper	3.45e12	7.8e-3
HOMc	HOM filter	Filter	Niobium		3e-2
		RF-seal gasket	Copper	3.45e12	7.8e-3

TABLE VII: Intrinsic quality factor Q_0 per HOM port when HOM filters are included, and associated power loss P_0 at nominal deflecting voltage $V_{t,nom}$ (3.4 MV)

III. MEASUREMENTS & RESULTS

A. Test I (Feb'17) – Bare DQW01

Scope

This was the first cryogenic RF test of a bare DQW SPS-series cavity.

Assembly

This test used the cavity DQW01. The thermosensor map was as follows: C-1, B-2, F-4 and A-5. Thermosensor #3 was located on the inner conductor blend, at the base of the FPC port. Thermosensors #6 and #7 were placed on the inner conductor blend, at the base of the HOMb and HOMc ports, respectively. Thermosensor #8 was located on the outer conductor blend, at the base of the FPC port.

Preparation

In preparation for this test, the cavity received the following surface treatment: bulk BCP, 600°C baking, light BCP, HPR and 120 °C degassing.

Results

The cavity quenched at 5.9 MV. Fig. 10 displays the $Q_0 - V_t$ curves measured during Test I. A first $Q_0 - V_t$ sweep found a soft multipacting band between 2–3 MV, that was easily conditioned. This multipacting band would never return back after the first break through. During the second sweep some field emitter blew up, and as evidence of that, for the third sweep the cavity reached slightly higher voltage with lower radiation levels. Most likely the quench was a magnetic quench. Operation in pulsed mode did not allow reaching higher voltages. At the quench field, the highest magnetic field in the cavity is at least 125 mT. This is a high magnetic field for an SRF cavity that followed a BCP-based surface treatment. Another evidence is found in the thermosensor signals.

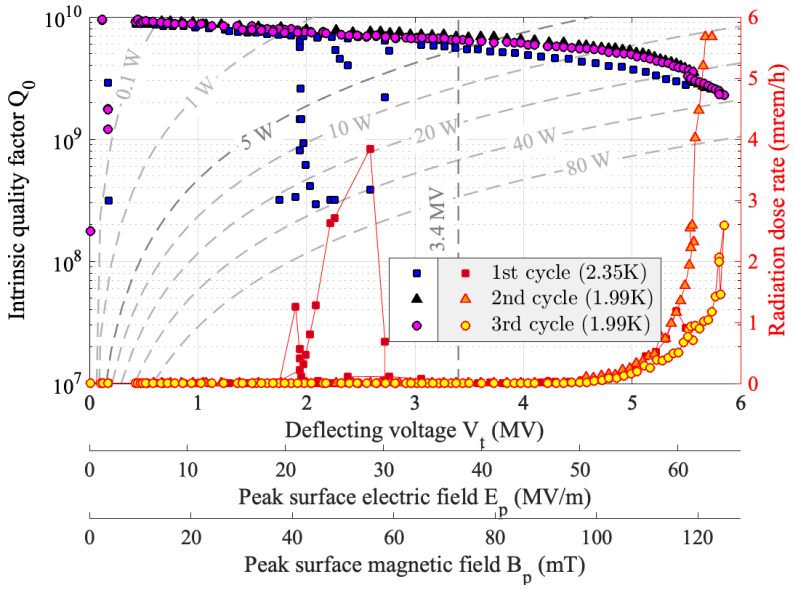

FIG. 10: $Q_0 - V_t$ curves for Test I (Feb'17) using DQW01.

The assembly experienced a Q-switch at 5.5 MV. The signal from thermosensor #2 increased abruptly at this field level, an indication that the Q-switch was associated to the niobium thin film deposited on the shortest small port (see Fig. 11). Temperature increases in other thermosensor locations (#6, #7 and especially #5) for fields higher than 5 MV until quench occurs. Thermosensor #5 corresponds to the region where the highest magnetic field in the cavity is expected, another indication that the quench is of magnetic nature.

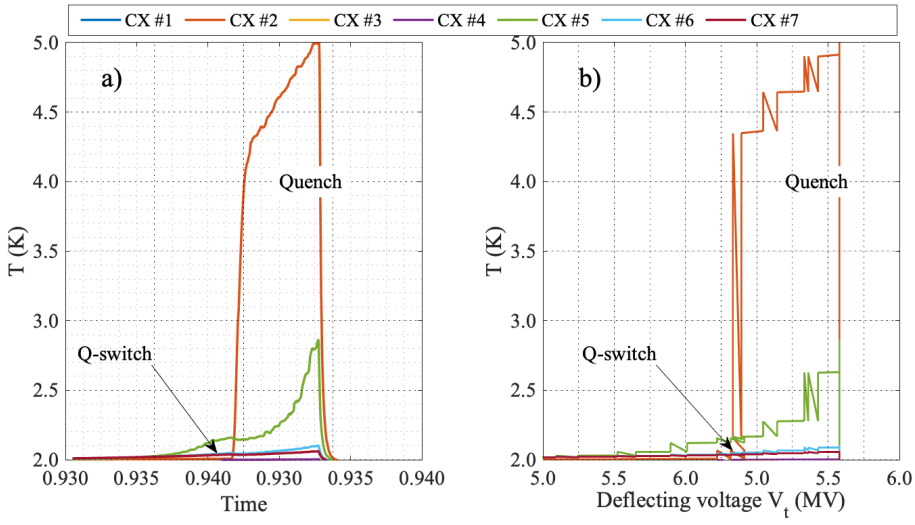

FIG. 11: Thermosensor signals for $Q_0 - V_t$ curves for Test I (Feb'17) using DQW01.

B. Test II (May'17) – Bare DQW01 with HOM01

Scope

This was the first cryogenic RF test of the a bare DQW cavity with an HOM filter.

Assembly

This test used cavity DQW01 with filter HOM01. The thermosensor map was as follows: C-1, B-2, F-4, A-5, D-7 and E-8. Thermosensor # 3 was placed on the flange that seals the HOM filter with the cavity, to monitor the gasket temperature. Thermosensor #6 was located by the HOMb port base, on the cavity-port blend.

Preparation

The hook region of the filter received a flash BCP in preparation for this test. The whole filter was rinsed by hand using pressurized water [20].

Results

The assembly quenched at 2.8 MV in CW mode and at 3.4 MV in pulsed mode. Figure 12 displays the $Q_0 - V_t$ curve measured at 2.0 K during Test II. The quench was not due to a hard field limit since operation in pulsed mode allowed reaching higher voltages.

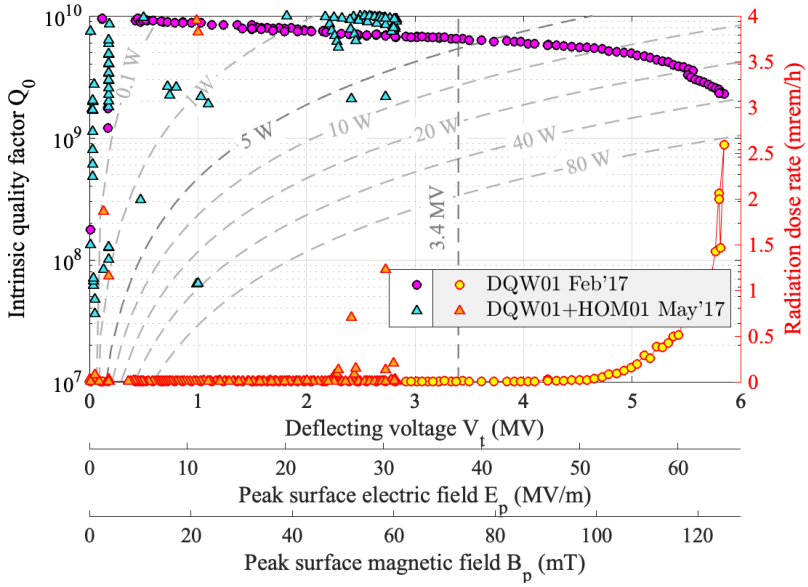

FIG. 12: $Q_0 - V_t$ curve for Test II (May'17) using DQW01 with HOM01.

The thermosensor signals support the idea that the performance was limited by a thermal quench. The quench at 2.8 MV was preceded by a small temperature increase on the coated flange of the shortest small port (thermosensor #5). The temperature also rose on one of the two thermosensors placed along the tube of the port where the HOM filter was installed (port HOMa) and on the thermosensors #7 and #8 located close to the cooling channel of the HOM filter. Thus, there were two possible thermal quench locations: the HOM hook or the coated flanges. The temperature increased dramatically in the highest magnetic field region (between ports HOMb and HOMc) every time that the cavity broke through the low-field multipacting band. This indicated that the hard field limit for a DQW SPS-series cavity equipped with HOM filters coincides with the high magnetic field expected for this region, the largest in the whole assembly.

A first multipacting barrier was found at about 0.1 MV. The conditioning continued for around 3 hours before the voltage jumped to about 1 MV. A soft barrier was found between 2–3 MV. It was easily processed and never came back after the first break through. The low-field band kept coming back, but could be processed easily by operating in pulsed mode or applying relatively higher power (tens of Watts) in CW mode [21]. Inspection of the decay signal showed no evidence of multipacting being the cause of the quench.

C. Test III (Jun'17)– Bare DQW02

Scope

This was the first cryogenic RF test of the bare cavity DQW02. The main scope of this test was to verify the repeatability of Test I (Feb.17) results.

Assembly

This test used cavity DQW02. The thermosensor map was as for Test I (Feb'17).

Preparation

In preparation for this test, the cavity received the following surface treatment: bulk BCP, 600°C baking, light BCP, HPR and 120 °C degassing.

Results

The field-emission onset appeared at 2.4 MV, leading to a pronounced Q-slope as the voltage increased. Operation was interrupted at 5.3 MV because the power necessary to run the cavity reached the administrative power limit. Figure 13 displays the $Q_0 - V_t$ curve measured at 2.0 K during Test III.

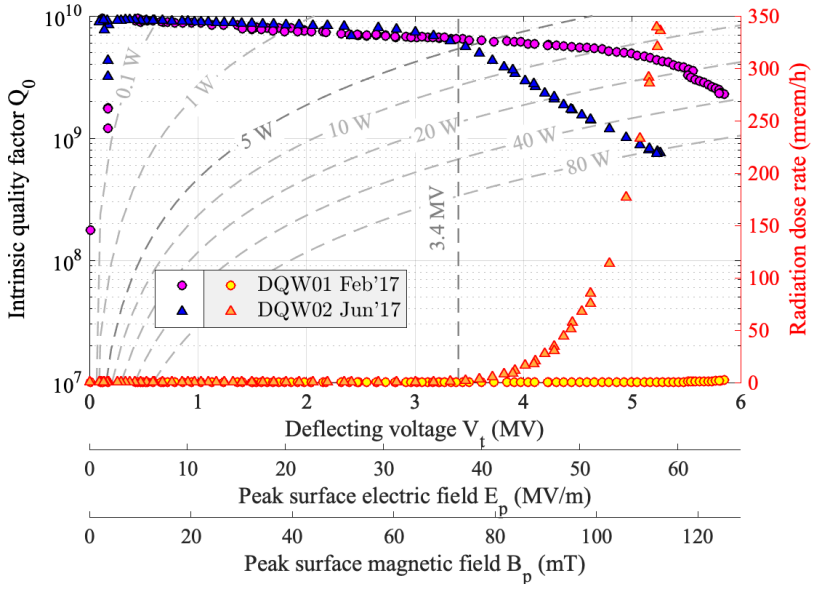

FIG. 13: $Q_0 - V_t$ curve for Test III (Jun'17) using DQW02.

All the thermosensors in the region around the cavity-port interface for ports HOMb and HOMc (#5-7) and for port HOMa (#4) monitored a temperature increase as soon as the voltage was larger than 4.7 MV. Fig. 14 shows the thermosensor signals for Test III. The cavity-port interfaces are high magnetic field regions in a DQW SPS-series cavity. The highest magnetic field is located between the ports HOMb and HOMc, at least 100 mT at 4.7 MV. The multipacting band between 2.3-3.0 MV was easily processed during a first sweep and did not appear for latter sweeps.

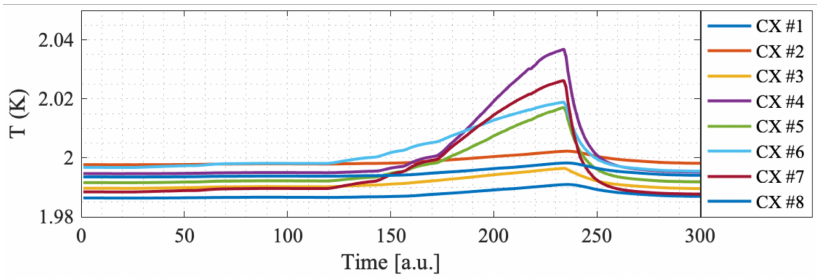

FIG. 14: Thermosensor signals for Test III (Jun'17) using DQW02.

D. Test IV (Sep'17) – Bare DQW02

Scope

The main scope of Test IV was to explore the maximum quench field that cavity DQW02 could provide. In the previous test (Test III in Jun'17), cavity DQW02 did not reach the ultimate performances observed with cavity DQW01 in Test I (Feb'17). The early field-emission onset and prominent Q-slope indicate that cavity DQW02 may have been contaminated. Thus, before testing cavity DQW02 again, its RF surfaces followed some light BCP and HPR.

Assembly

This test used cavity DQW02. The thermosensor location changed from previous tests. The thermosensor map for Test IV was as follows: C-1, B-3, F-4 and A-7. Thermosensor #2 was placed on top of the Nb-coated, zero-length flange of the longest beam port, where the vacuum line is connected. The flange used for this connection had a scratch in the Nb thin film. Thermosensor #6 was positioned by the HOMa port base, on the outer conductor blend and thermosensor #8 was placed near the highest magnetic field spot, on the outer conductor blend. Spatter and sharp welds were found before bulk BCP in those locations [22], as shown in Fig. 15.

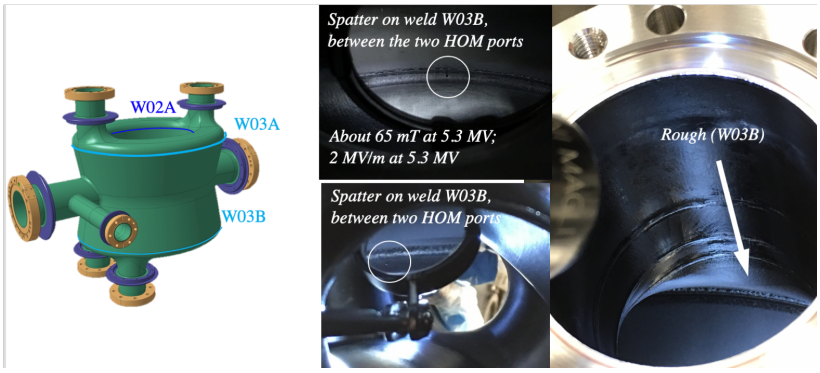

FIG. 15: Weld map for a DQW SPS-series cavity and features found on the RF surface of cavity DQW02 during visual inspection performed before bulk BCP.

Preparation

Cavity DQW02 received some light BCP, HPR and 120°C bake prior to Test IV.

Results

The assembly quenched at 5.3 MV. The field-emission onset appeared at 3.4 MV, at higher voltages than for the previous test, but still led to a steep Q-slope. The heat load decreased, being within the specifications – below 5 W at nominal deflecting voltage (3.4 MV). Figure 16 displays the $Q_0 - V_t$ curve measured at 2.0 K during Test IV. Table VIII summarizes the main results of this test.

Only thermosensors #1 (on the shortest beam port flange, where the input probe is installed) and #7 (on the highest magnetic field region in the whole assembly) show a temperature increase during Test IV. The thermosensor signals are shown in Fig. 17. When the quench field is reached, at 5.3 MV, thermosensor #1 displays higher temperature than #7. As the voltage is decreased, the temperature registered by both thermosensors decreases. Thermosensor #1 founds a larger temperature for a longer time after quench than #7. The thermal path from the helium bath to the niobium thin film deposited on the stainless-steel flange of the short beam port is longer than for point #7. Thus, longer time is also expected for the film to become superconducting again after quench.

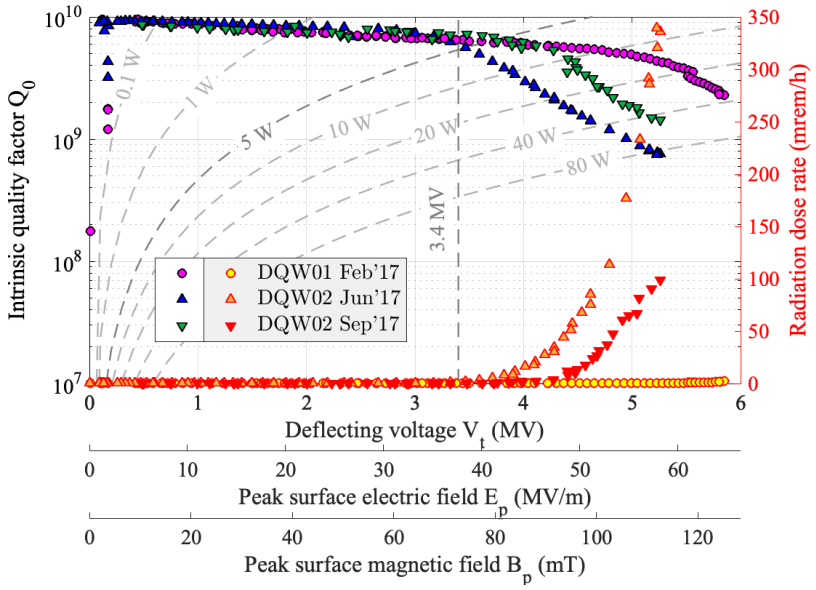

FIG. 16: $Q_0 - V_t$ curve for Test IV (Sep'17) using DQW02.

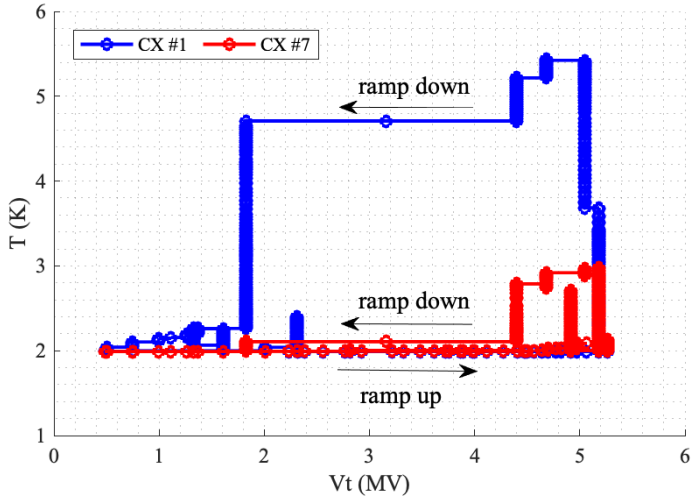

FIG. 17: Thermosensor signals for Test IV (Sep'17) using DQW02.

E. Test V (Oct'17) – Bare DQW02 with HOM01

Scope

The scope of this test was to evaluate the performances of a DQW cavity equipped with an HOM filter. The first and last test of a DQW cavity with an HOM filter (Test II in May'17) found an early quench at 2.8 MV, attributed to insufficient surface treatment.

Assembly

Tests with the HOM filter continued with cavity DQW02 instead of cavity DQW01. This test employed cavity DQW02 and filter HOM01. The thermosensor map was as follows: C-1, B-2, F-4, A-5, D-7 and E-8. Thermosensor #3 was positioned closed to the flange in port HOMa and #6 by the base of port HOMb, on the inner conductor blend.

Preparation

Cavity DQW02 received some light BCP and HPR; the filter HOM01 received some local flash BCP (on the hook region) followed by an ultrasonic cleaning bath prior to installation into cavity DQW02. The assembly was degassed at 120°C.

Results

The cavity reached 3.6 MV in CW mode, and 4.12 MV in pulsed mode [23]. The performance improvement with respect to Test II (May'17) was attributed to the additional surface treatment followed by the HOM filter. Figure 18 displays the first $Q_0 - V_t$ curve measured at 2.0 K during Test V. Thermosensor #4, at the base of port HOMa on the inner conductor blend, showed the largest response to the voltage increase. Thermosensors #7 and #8, close to the cooling channel of the HOM filter, also showed a temperature increase for large voltage values. Table VIII summarizes the main results of this test.

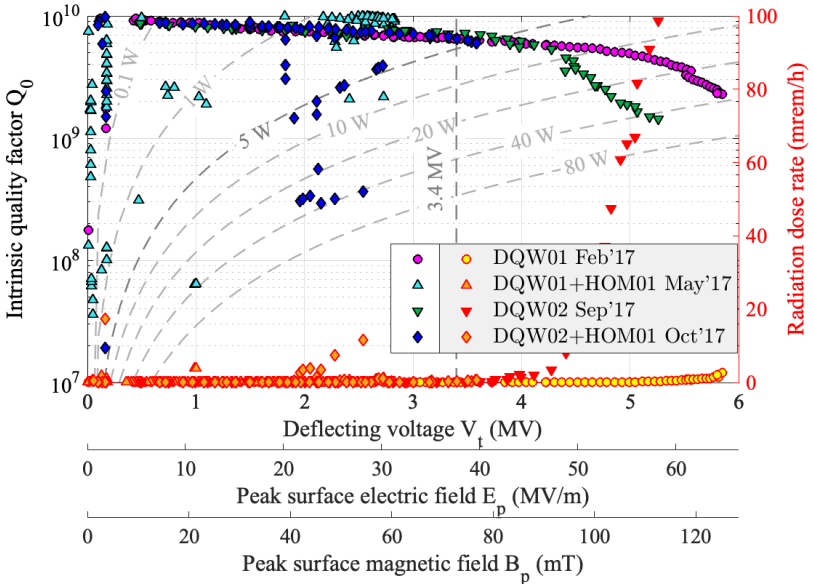

FIG. 18: First $Q_0 - V_t$ curve for Test V (Oct'17) using DQW02 with HOM01.

A hard multipacting band was found between 0.15–0.2 MV. Conditioning required a large incident power of about 75 W and operation in pulsed mode. The multipacting band was broken through after 4 hours. The cavity would fall back into this hard multipacting band afterwards, but its conditioning took shorter times of less than 10 minutes. Some other multipacting bands were found: a low-field multipacting band between 0.065–0.088 MV, and high-field band between 1.8–2.3 MV. These soft zones were easy to condition and did not return after the first break through. All these multipacting bands also appeared in the bare cavity cold tests.

During multipacting conditioning, field broke through the multipacting band and suddenly jumped reaching a very high voltage, what may have blown up a field emitter. In the successive sweeps, the cavity performance was field-emission dominated. Figure 19 compares the two $Q_0 - V_t$ curves measured at 2.0 K during Test V. This situation remained unnoticed after Test VI (Jan'18) was conducted.

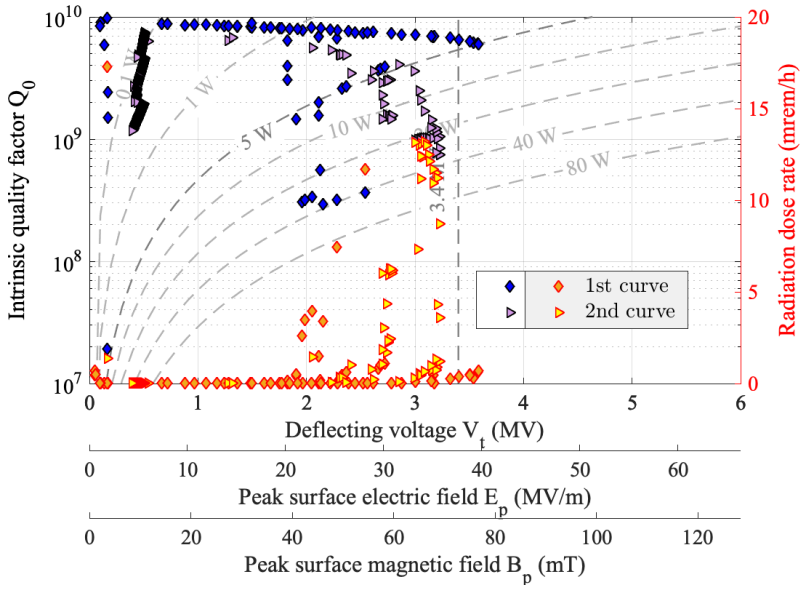

FIG. 19: First and second $Q_0 - V_t$ curves for Test V (Oct'17) using DQW02 with HOM01.

F. Test VI (Jan'18) – Bare DQW02 with HOM01

Scope

Test V (Oct'17) reached larger voltages than what was achieved in Test II (May'17). This improvement was associated to the additional local flash BCP received by the HOM filter. The scope of this test was to evaluate the impact on performance when providing additional surface treatment to the filter, in search for the ultimate performances of a DQW cavity with an HOM filter.

Assembly

This test used the same assembly as for Test V (Oct'17). The thermosensor map was as follows: C-1, B-2, F-4,6, D-7 and E-8. Thermosensors #3 and #5 were by the flange of port HOMa.

Preparation

The HOM filter was treated as follows: bulk BCP (100 µm), 600° baking, light BCP and manual pressure rinsing.

Results

The assembly performance was characterized by an early field-emission onset and a pronounced Q-slope at medium fields. The performance for Test V (Oct'17) and Test VI (Jan'18) shows a similar early Q-slope accompanied with large radiation. Figure 20 displays the $Q_0 - V_t$ curve measured at 2.0 K during Test VI.

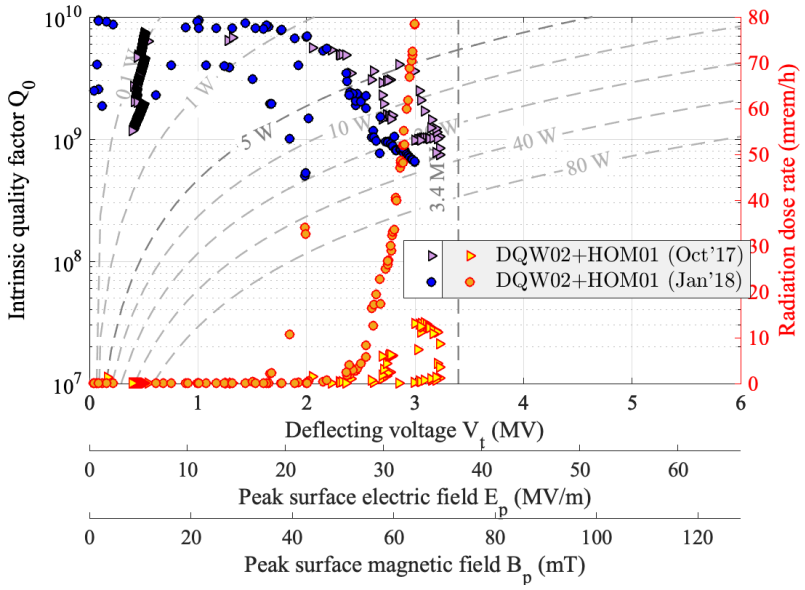

FIG. 20: $Q_0 - V_t$ curve for Test VI (Jan'18) using DQW02 with HOM01.

G. Test VII (May'18) – Bare DQW02 with HOM01

Scope

The previous test did not tell if the quench was related to the DQW cavity or the HOM filter. The performance was field-emission dominated for Test V (Oct'17) and Test VI (Jan'18). Therefore, for this test the cavity went through HPR. In addition, the HOM filter may have suffered from HFQS, as bulk BCP was performed on the HOM filter between Test V (Oct'17) and Test VI (Jan'18) but the filter was not baked. Thus, the HOM filter was also baked at 120°C.

Assembly

This test used cavity DQW02 and filter HOM01. The thermosensor map was as follows: C-1, B-2, F-4,6, D-7 and E-8. Thermosensors #3 and #5 were by the flange of port HOMa.

Preparation

The cavity underwent HPR, while the HOM filter was manually rinsed with pressurized water. Then, the whole assembly was degassed at 120°C for 24 h.

Results

The assembly quenched at 4.7 MV with barely no field emission before the quench field was reached. This was the largest voltage ever achieved by the assembly of a DQW SPS-series cavity and its HOM filter. This excellent performance is attributed to adequate surface treatment applied to cavity and HOM filter. Figure 21 displays the $Q_0 - V_t$ curve measured at 2.0 K during Test VII. The $Q_0 - V_t$ curve for this test showed higher Q at 4.7 MV than for Test IV (Sep'17) with cavity DQW02 by itself and is comparable to the Q found for Test I (the best data set for a bare DQW cavity). An array of Oscillating Superfluid Transducers (OST) was installed around the assembly. Unfortunately, data could not determine the origin of the quench.

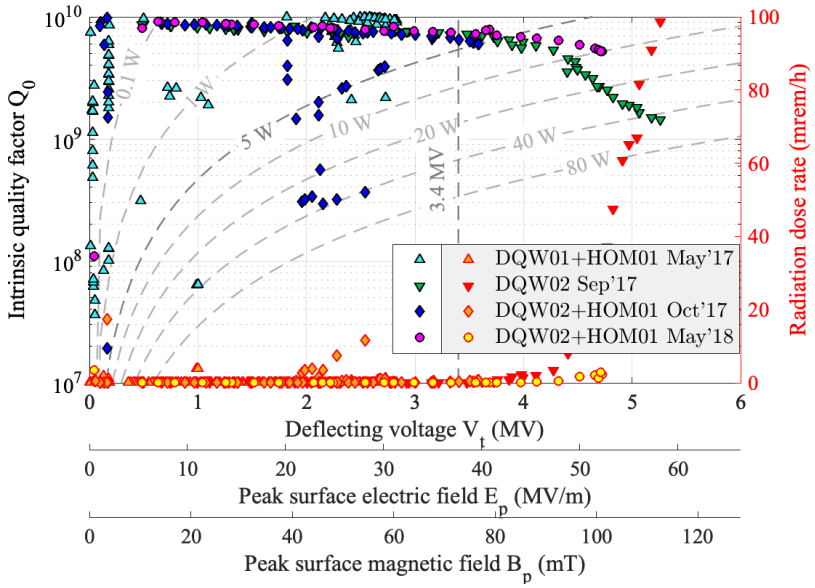

FIG. 21: $Q_0 - V_t$ curve for Test VII (May'18) using DQW02 with HOM01.

H. Test VIII (Jul'18) – Bare DQW02 with HOM01 separated by NbTi spacer

Scope

With the scope of discriminating the location of the quench, an NbTi spacer retracted the HOM filter further away from the cavity. By retracting the filter out from the cavity, it was exposed to lower magnetic fields. If the quench was related to the cavity or to the system cavity-filter, the retraction of the HOM filter would not allow higher voltages to be reached. If the quench was related to the HOM filter (due to the hard field limit being reached in the filter – magnetic quench – or because the power dissipated was such that the cooling was insufficient – thermal quench), the retraction would decrease the magnetic field, and higher fields could be reached.

Assembly

This test used cavity DQW02 and filter HOM01. The HOM filter was retracted from the cavity by a 20 mm long NbTi spacer. No thermosensor data was taken for this test.

Preparation

The cavity underwent HPR, while the HOM filter was manually rinsed with pressurized water. Then, the whole assembly was degassed at 120°C for 24 h.

Results

The external Q for the pickup probe (Q_e) was one order of magnitude larger than for previous tests. Fig. 23 displays the Q_0-V_t curve measured at 2.0 K during Test VIII. If the Q_e value is trusted, the maximum magnetic field in the assembly would be larger than 150 mT. Up to our knowledge, this is an unprecedented field for a SRF cavity that has received a BCP-based treatment. On the other hand, the maximum electric field would be larger than 80 MV/m. This value exceeds the Kilpatrick limit by more than a factor 4 but barely no field emission observed.

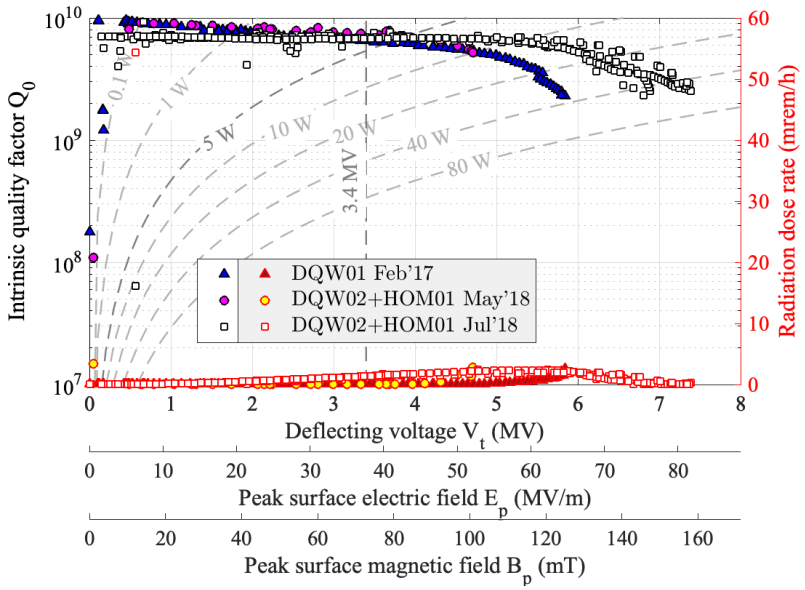

FIG. 22: $Q_0 - V_t$ curve for Test VIII (Jul'18) using DQW02 with HOM01 separated by NbTi spacer.

Swapping the cable readouts assigned to the pickup probe and the HOM filter output leads to the results depicted in Fig. 23, which seem more reasonable than those from Fig. 22 and find the same quench field as for Test I (Feb.'17) involving only the bare cavity. If this was the case, the cavity DQW02 would have reached, for the first time, the same high quench field as cavity DQW01.

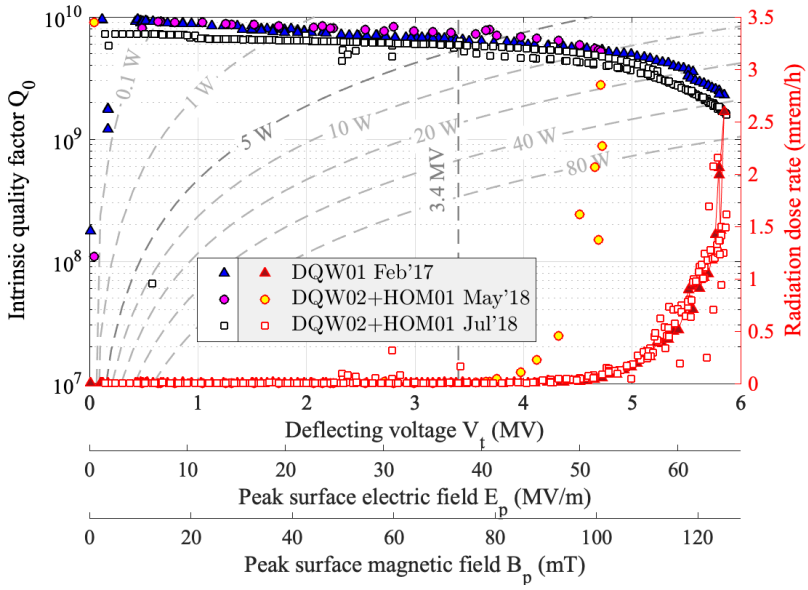

FIG. 23: $Q_0 - V_t$ curve for Test VIII (Jul'18) using DQW02 with HOM01 separated by NbTi spacer.

I. Test IX (Sep'18) – Bare DQW02 with HOM01 separated by NbTi spacer

Scope

Evaluate the performances of the Test VIII (Jul'18) assembly after high-pressure rinsing the cavity to eliminate any possible contaminant.

Assembly

The same as for Test VIII (Jul'18). The thermosensor map was as follows: B-1, C-2, D-7, E-8, F-4, and A-5, Thermosensor #3 was close to the gasket in the port HOMa and #6 was on the inner conductor blend by the port HOMb.

Preparation

Cavity DQW02 followed HPR and then the whole assembly baked at 120°C in preparation for this test.

Results

Two $Q_0 - V_t$ curves were taken for Test IX. Figure 24 displays the first $Q_0 - V_t$ curve measured at 2.0 K during Test IX. The quench field was 5.1 MV, close to the value obtained in Test IV (Sep'17) for the bare cavity DQW02. Table VIII summarizes the main results of this test. By retracting the HOM filter about 20 mm – which decreases the fields in the HOM filter by a factor 2 – the quench field was sooner reached in the cavity rather than the HOM filter. A Q-switch appears for voltages between 1.2 – 1.6 MV, lowering the Q_0 at higher voltages.

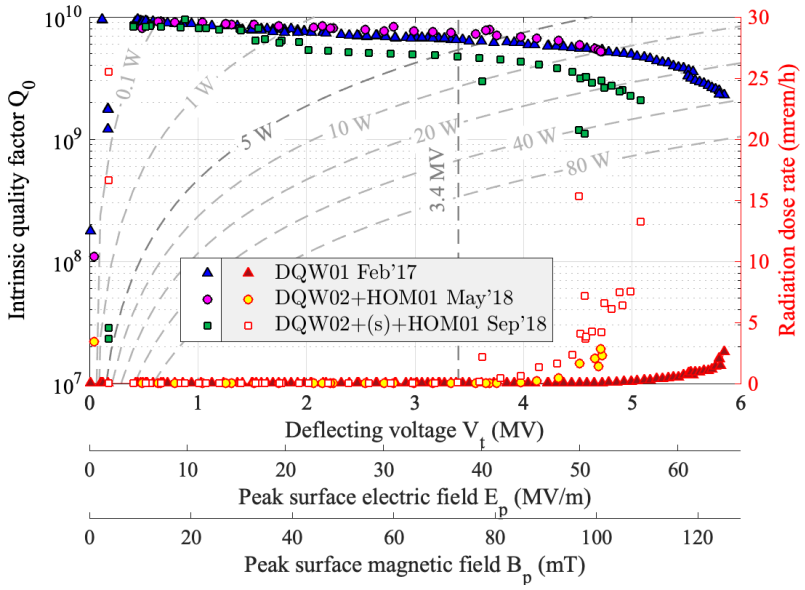

FIG. 24: First $Q_0 - V_t$ curve for Test IX (Sep'18) using DQW02 with HOM01 separated by NbTi spacer.

Figure 25 shows the performance evolution during Test IX. The performance seems to deteriorate after the first $Q_0 - V_t$ curve (more pronounced HFQS driven by larger field-emission current, earlier quench). The blow-up of an emitter could explain this deterioration. Thermosensor #3 was not available during the voltage sweep. Thermosensor #8 (in the HOM filter, by its cooling channel) followed the voltage profile until it got lost; however, thermosensor #7 did not registered any temperature increase. The other thermosensors did not show any significant temperature increase during the test. Fig. 26 shows the thermosensor signals collected during Test IX.

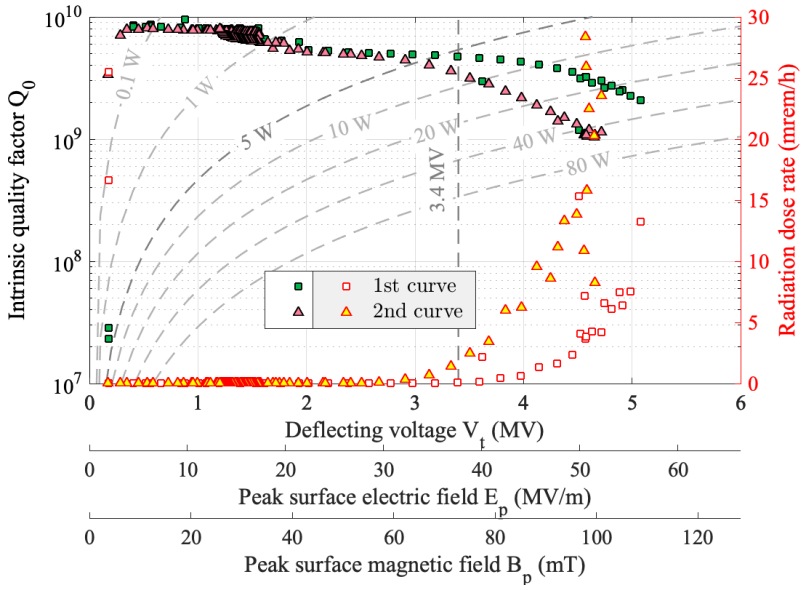

FIG. 25: Comparison between the two $Q_0 - V_t$ curves for Test IX (Sep'18) using DQW02 with HOM01 separated by NbTi spacer.

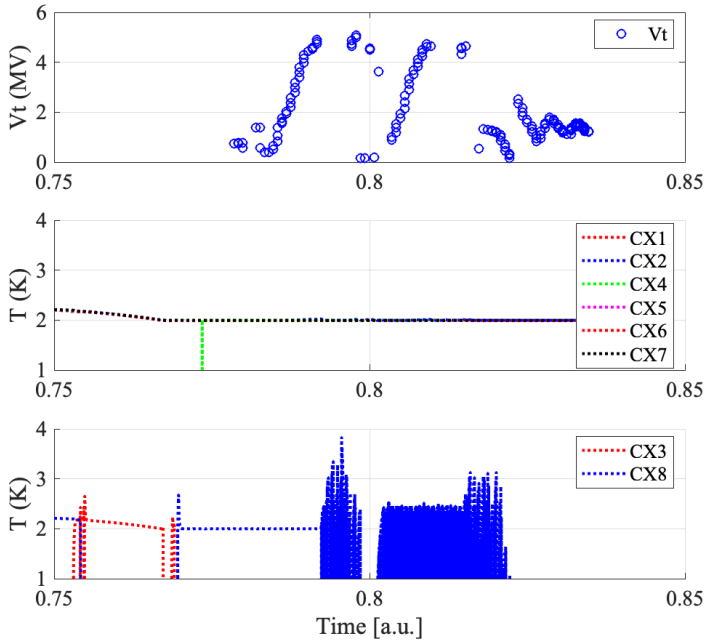

FIG. 26: Thermosensor signals for Test IX.

J. Test X (May'19) – DQW02 with HOM01

Scope

The main scope of Test X was to verify the repeatibility of Test VII results (early quench at 4.7 MV), to exclude that higher quench field observed for Test VIII and Test IX is not exclusively related to the additional HPR followed by the cavity in preparation for these two tests.

Assembly

The assembly consisted of DQW02 and HOM01 (as for Test VII). The thermosensor map was as follows: B-1, C-2, F-4, D-7 and E-8. Thermosensor #3 was placed on the HOMa port, close to the gasket. Thermosensor #5 was placed inside the cooling channel of the HOM filter. Thermosensor #6 was placed between #3 and #4.

Preparation

The RF surfaces did not receive any additional surface treatment after Test IX in preparation for Test X.

Results

The assembly reached 4.5 MV before quench. Figure 27 displays the $Q_0 - V_t$ curves measured at 2.0 K during Test X. Table VIII summarizes the main results of this test. The quench field for Test X was found at lower values than for Test VII (May'18). Fig. 28 shows the evolution of the radiation level with voltage for different tests of the DQW02 cavity. From Test VII (May'18) to Test IX (Sep'18), the field-emission onset moved to lower voltages. Test X also showed a low field-emission onset with respect to Test VII (May'18).The change in slope between the two $Q_0 - V_t$ curves taken during Test X (the earlier with a field emission onset at 1.6 MV; the latter, at 2.1 MV) may be an indication of an emitter blowing up. The latter curve finds a field-emission onset similar to previous values observed after Test VII (May'18). Note that the assembly was not high-pressure rinsed in preparation for Test X and some contamination may have occurred during removal of the NbTi spacer.

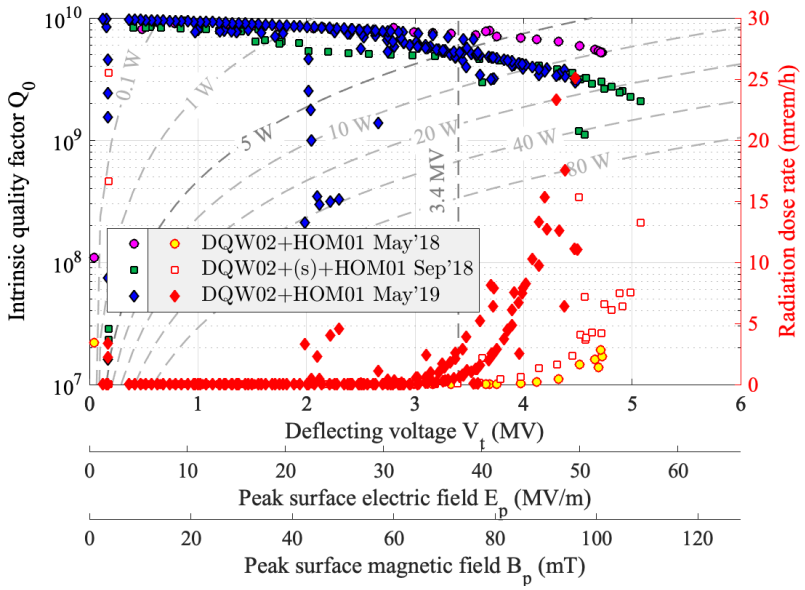

FIG. 27: $Q_0 - V_t$ curves for Test X (May'19) using DQW02 with HOM01 after removal of NbTi spacer.

The 1st $Q_0 - V_t$ curve taken for Test X found a multipacting band for voltages between 2 and 3 MV, conditioned before the 2nd curve was taken, as seen in Fig. 29 and 28. The assembly experienced a Q-switch around 2.5 – 3.5 MV, which was accompanied by a slight temperature increase in all the thermosensors, with the largest increase being recorded for #5 (in the HOM filter, inside its cooling channel). The quench was paired with a slight temperature increase in thermosensors #1 (on the FPC flange - the largest temperature increase), #5 (in the HOM filter, inside its cooling channel) and #7 (in the HOM filter, by its cooling channel). Fig. 30 displays the thermosensor signals collected during Test X.

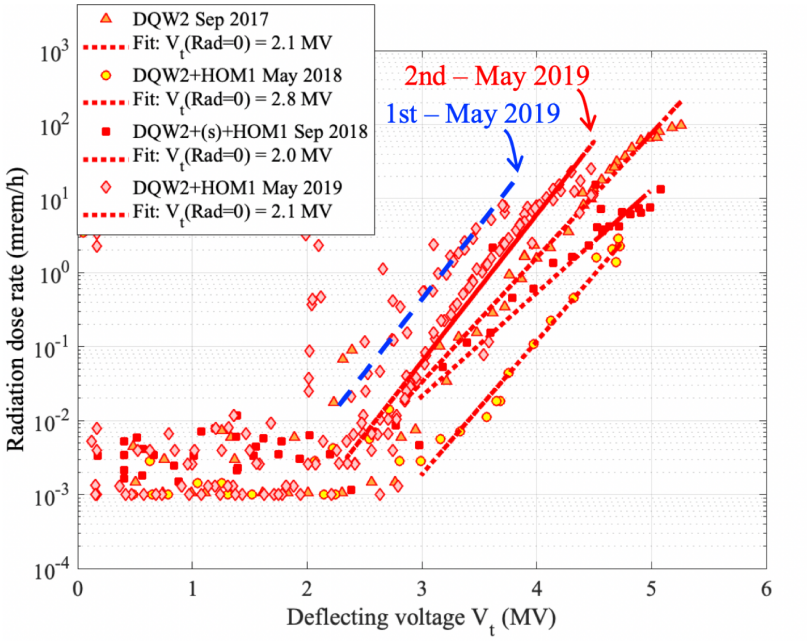

FIG. 28: Radiation evolution for some tests employing the cavity DQW02.

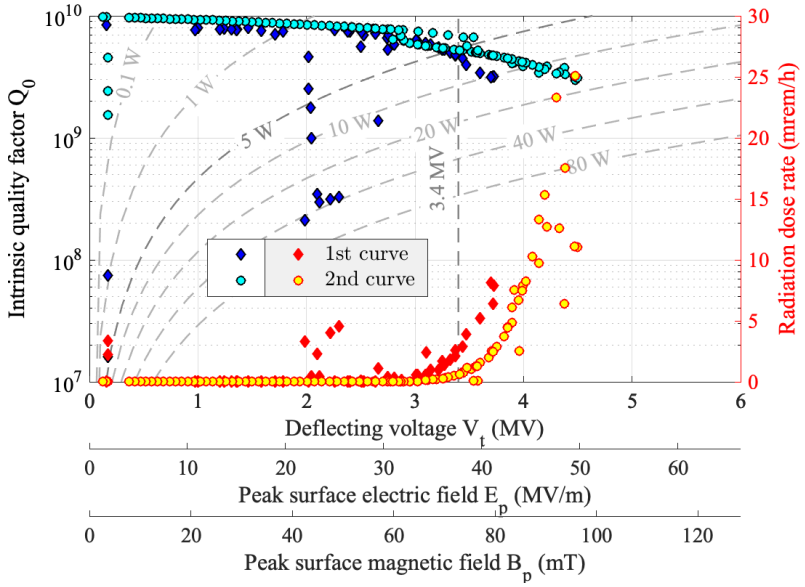

FIG. 29: Comparison between $Q_0 - V_t$ curves for Test X (May'19) using DQW02 with HOM01 after removal of NbTi spacer.

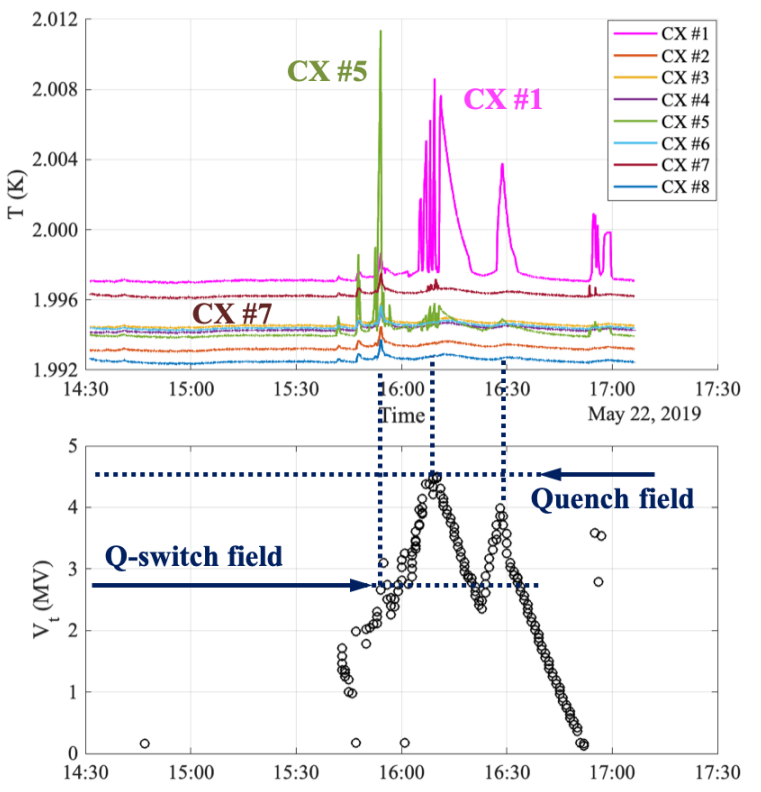

FIG. 30: Thermosensor signals for Test X.

K. Test XI (Jul'19) – DQW02 with HOM01 and HOM02

Scope

The scope of this test was to evaluate the performance of the DQW SPS-series design when more than one HOM filter is assembled to the cavity. This configuration is closer to the final one, with 3 HOM filters assembled to the cavity.

Assembly

The filter HOM02 was installed in the bottom port HOMb, withstanding 45 degrees with respect to the vertical beam plane, as designed for the final setup of the fully dressed DQW SPS-series cavity. Fig. 31 shows the cavity DQW02 with the filter HOM02 installed in port HOMb. For this test, the pickup probe was borrowed from DQW01 because the pickup probe from DQW02 broke. The thermosensor map was as follows: B-1, C-2, G-3, H-4, A-5, F-6, D-7 and E-8.

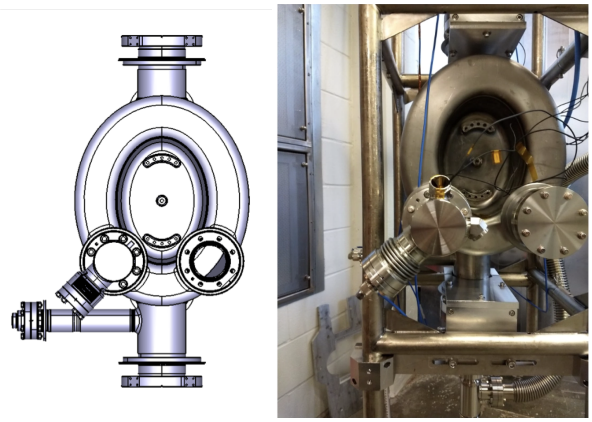

FIG. 31: Orientation of filter HOM02 installed in port HOMb for Test XI (Jul'19).

Preparation

The filter HOM02 went through the following surface preparation before the test: heavy BCP (100 µm) done in two iterations, baking at 600°C for 10 hours, light BCP (10 µm) and ultrasound cleaning. The cavity went through HPR. Then the whole assembly was backed at 120°C.

Results

Figure 32 displays the $Q_0 - V_t$ curve measured at 2.0 K during Test XI. The test was stopped when the deflecting voltage in the cavity was about 2.8 MV because the power coming through the filter HOM02 reached the administrative limit. At 2.8 MV, the power coming through the filter HOM02 was 9 W, to be compared with the 0.2 W for the filter HOM01. A possible explanation for such large power transmission is that the notch of filter HOM02 was detuned with respect to the cavity frequency, so either the filter HOM02 or the cavity need to be tuned. Such large power coming through the filter may also explain why the external Q of the pickup probe $\left(3.4 \times 10^{13}\right)$ is one order of magnitude higher than for other tests.

The field emission onset appears earlier than for the previous test, at 1.4 MV. This might be an indication that the filter HOM02 required the hand pressurized rinsing that was skipped in preparation for this test. Table VIII summarizes the main results of this test.

The assembly was inspected after this cold test, finding that the pickup probe was loose. This may explain the higher external Q of the pickup port.

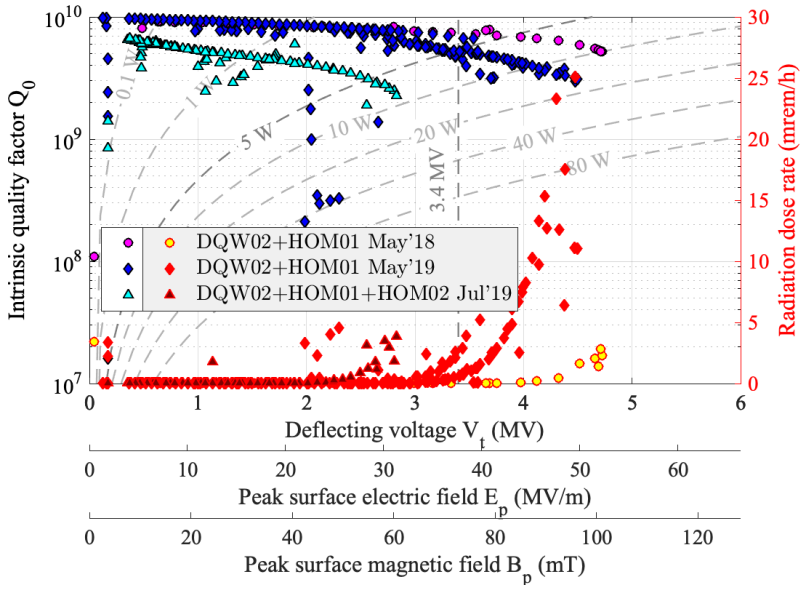

FIG. 32: $Q_0 - V_t$ curve for Test XI (Jul'19) using DQW02 with HOM01 and HOM02.

L. Test XII (Oct'19) – DQW02 with HOM01 and rotated HOM02

Scope

The scope of this test was a second attempt to evaluate the performance of the DQW SPS-series design when more than one HOM filter is assembled to the cavity. This configuration is closer to the final one, with 3 HOM filters assembled to the cavity. The previous test showed large fundamental mode power leaking from filter HOM02. For this test, the filter HOM02 has been rotated with respect to the design orientation to present a larger external Q at the fundamental mode frequency.

Assembly

The filter HOM02 was installed in the bottom port HOMb, withstanding 90 degrees with respect to the vertical beam plane, as shown in Fig. 33, for a target external Q of 10^{11}. The quality assurance measurements performed with the cavity under vacuum and at room temperature found an external Q of $6.441e10$ for the HOMa port hosting the HOM01 filter and $2.032e11$ for the HOMb port with the HOM02 filter rotated. The feedthrough of the input port was borrowed from cavity DQW01 because the one from DQW02 was damaged. The thermosensor map was as follows: B-1, C-2, G-3, H-4, A-5, F-6, D-7 and E-8.

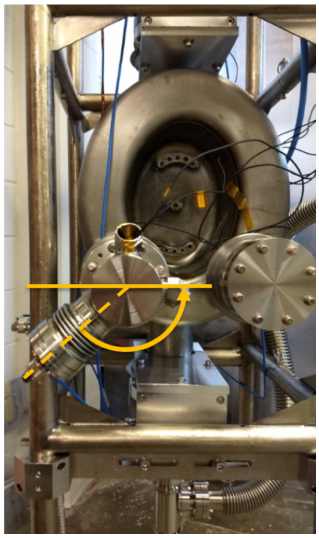

FIG. 33: Orientation of filter HOM02 installed in port HOMb for Test XII (Oct'19).

Preparation

Both filters, HOM01 and HOM02, went through pressurized hand-held water rinsing followed by ultrasound cleaning. The cavity was high-pressure rinsed. Then, the whole assembly was leak tested and backed at 120°C.

Results

The assembly quenched at 4.0 MV during CW operation. The field-emission onset appeared at low fields, around 2 MV, as already seen for other cryogenic RF tests of a DQW cavity with HOM filters. This early field-emission onset may be the cause for the quench at 4.0 MV. Fig. 34 displays the $Q_0 - V_t$ curve measured at 2.0 K during Test XII and Table VIII summarizes the main results of this test.

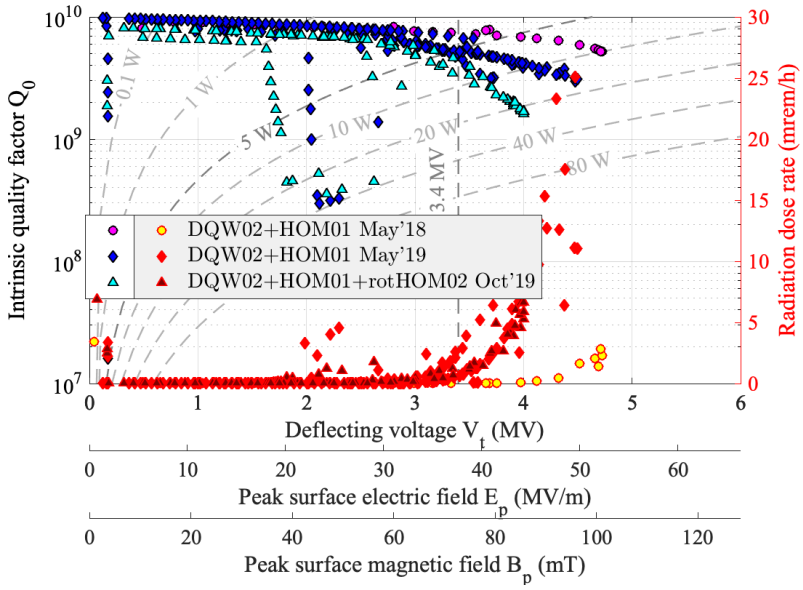

FIG. 34: $Q_0 - V_t$ curve for Test XII (Oct'19) using DQW02 with HOM01 and rotated HOM02.

IV. DISCUSSION

A summary of the tests conducted with the LARP DQW SPS-series cavities is presented in Table VIII. The following section is dedicated to discuss the main observations from the series of tests conducted with the LARP DQW SPS-series prototypes.

A. Bare Cavities

The bare DQW SPS-series cavities exceeded nominal deflecting voltage (3.4 MV) with up to 73% margin and the heat load was lower than 10 W as required at 4.1 MV. The cavities presented an excellent performance beyond nominal deflecting voltage up to 5.9 MV, showing pretty low RF surface resistance (9 nOhm) and reaching high electric and magnetic fields (up to 65 MV/m and 125 mT, respectively) with a field-emission onset at voltages above the nominal deflecting voltage.

The performance of cavity DQW02 during its bare cavity tests seems not optimal due to field emission — evidenced by much lower Q_0 and higher radiation than DQW01. However, the maximum magnetic field reached by cavity DQW01 and DQW02 is comparable when errors are accounted. On the other hand, if the results displayed in Fig. 23 for Test VIII (Jul'18) are trusted, cavity DQW02 would have actually reached the same quench field as the cavity DQW01 in Test I (Feb'17). Thus we can make the claim that the performance of both cavities is comparable and the results are reproducible.

The quench for both bare cavities is of magnetic nature. Data collected for both cavities (DQW01 for Test I in Feb'17 and DQW02 for Test III in June'17 and Test IV in Sep'17) shows that the temperature around ports HOMb and HOMc was higher for voltages over 5 MV. This is the highest magnetic field region in the whole assembly, with the field being at least 107 mT for a deflecting voltage of 5 MV. At quench field, the maximum magnetic field (about 125 mT) is equivalent to a TESLA single-cell cavity delivering 30 MV/m [24]. Another evidence were the fast quenches and associated temperature increase in the highest magnetic field region after sudden passage of multipacting bands.

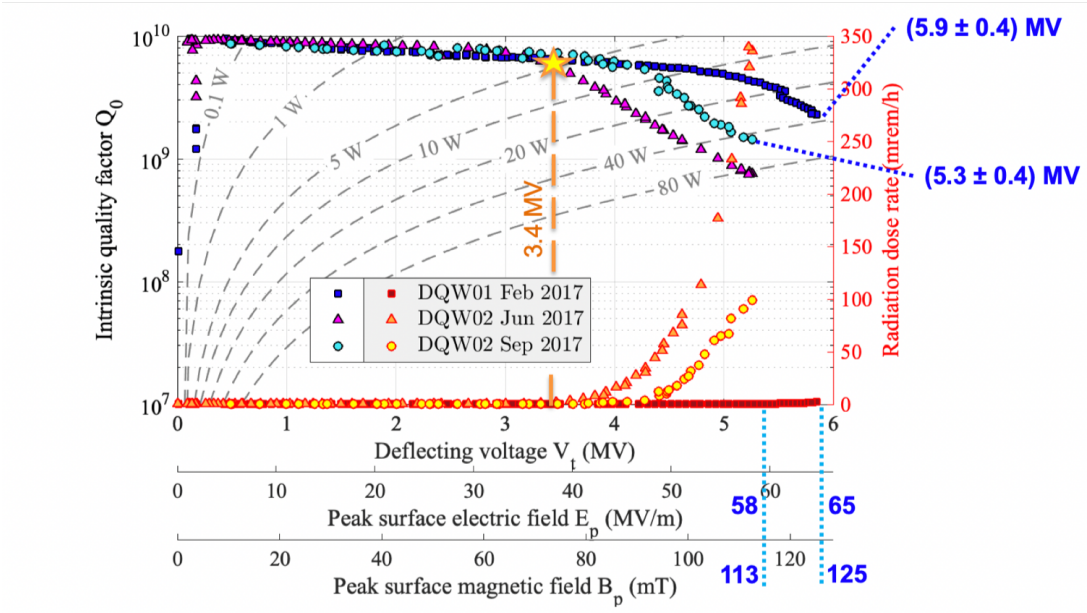

FIG. 35: Q_0 vs V_t curves for collection of bare cavity tests. The yellow star marks the target of 5 W heat load maximum at 3.4 MV.

B. Dressed Cavities: Bare Cavities with HOM Filters

The performances for DQW SPS-series cavities equipped with HOM filters were limited at earlier voltages (4.5–4.7 MV) by quench than for bare cavity tests. Still, they reached well beyond the required nominal deflecting voltage with a comfortable margin of 38%. In addition, reproducibility was confirmed (see Test VII in May'18 and Test X in May'19). The quench experienced by the dressed DQW cavities was sharp, but not necessarily accompanied by a significant radiation increase or multipacting (the closest multipacting band appears between 2–3 MV). The test campaign was complemented with simulation-based studies to fully understand the limiting factor in the performance of the dressed DQW cavities.

Test	Assembly	Surface preparation		Max. V_t (MV)	FE onset (MV)	$Q_{0,low}$	$Q_{0,nom}$ [P (W)]	CERNOX with temperature increase	LFD (Hz/(MV)^2)
		Cavity	HOM filter						
Test I (Feb'17)	DQW01	Bulk BCP, 600°C, light BCP, HPR, 120°C	n/a	5.9	4.1	1e10	6e9 [4.5]	B-2, F-4	
Test II (May'17)	DQW01+HOM01 Flange set b	None	Flash BCP (on hook); rinse	2.8	n/a	1e10	n/a	B-5, D-7, E-8	-450
Test III (Jun'17)	DQW02	Bulk BCP, 600°C, light BCP, HPR, 120°C	n/a	5.3	2.4	9e9	5.9e9 [4.6]	A-567, F-4	
Test IV (Sep'17)	DQW02	Light BCP, HPR, 120°C	n/a	5.3	3.4	1e10	6.5e9 [4.2]	C-1, A-7	-554
Test V (Oct'17)	DQW02+HOM01 Flange set a	Light BCP, HPR, 120°C	Flash BCP (on hook); US bath, 120°C	3.6	n/a	1e10	6.3e9 [4.3]	F-4, D-7, E-8	-499
Test VI (Jan'18)	DQW02+HOM01 Flange set a	None	100 µm BCP, 600°C, light BCP, rinse	3.1	2.6	1e10	n/a	–	-599
Test VII (May'18)	DQW02+HOM01 Flange set a	HPR, 120°C	Rinse, 120°C	4.7	3.2	1e10	7.6e9 [3.5]	–	-772
Test VIII (Jul'18)	DQW02+HOM01 + NbTi spacer Flange set a	HPR, 120°C	Rinse, 120°C	5.9	4.1	8e9	5.8e9 [4.6]	–	
Test IX (Sep'18)	DQW02+HOM01 + NbTi spacer Flange set a	HPR, 120°C	None	5.1	2.4	9e9	4.7e9 [5.7]	E-8	
Test X (May'19)	DQW02+HOM01 Flange set a	None	None	4.5	2.8	1e10	6e9 [4.5]	C-1, F-5, D-7	-700
Test XI (Jul'19)	DQW02+HOM01 +HOM02 Flange set a	HPR, 120°C	Bulk BCP, 600°C, light BCP, US bath, 120°C	2.8	1.5	6.2e9	n/a	n/a	-742
Test XII (Oct'19)	DQW02+HOM01 +rotHOM02 Flange set a	HPR, 120°C	Rinse, 120°C	4.0	2.4	8e9	4e9 [6.7]	n/a	–

TABLE VIII: Summary of LARP DQW SPS-series cryogenic RF tests

1. *Effect of surface treatment followed by HOM filter*

All the HOM filters tested before Test VI (Jan'18) had received a minimal surface treatment consisting of flash (20 µm) Buffered-Chemical Polishing (BCP) exclusively in the hook section and manual pressure rinsing. The insufficient surface treatment followed by the HOM filters was the main cause of the early quench, as shown by the higher voltages achieved by subsequent improvement of the filter RF surface between Test V (Oct'17) and Test VII (May'18) (see Table II). With a complete surface treatment including bulk BCP (only on the hook, where the magnetic field is the highest in the whole HOM filter), high-temperature (600°C) degassing and low-temperature (120°C) baking, the cavity plus filter assembly could reach 4.7 MV with no evidence of High-Field Q-Slope (HFQS).

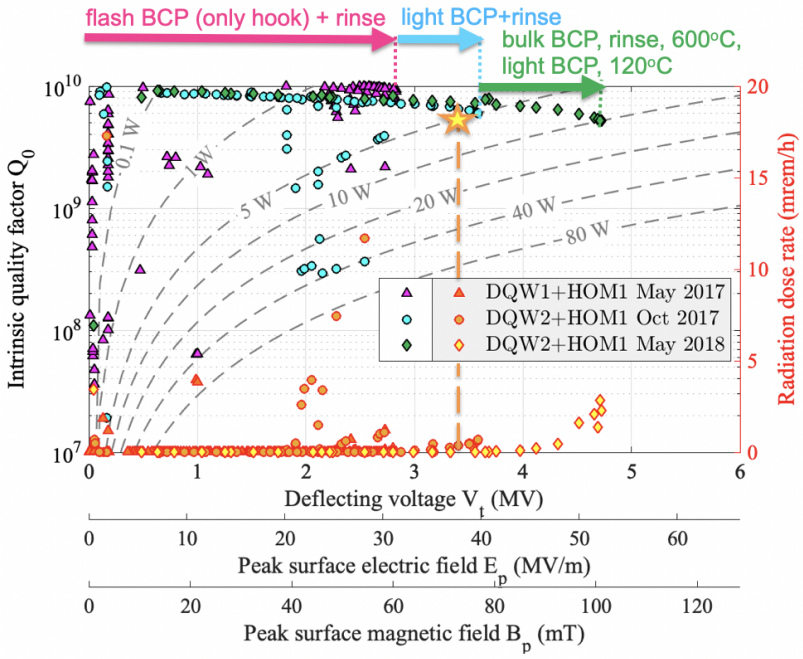

FIG. 36: Q_0 vs V_t curves for collection of tests illustrating the effect of surface treatment applied to HOM filter on cavity performance. The yellow star marks the target of 5 W heat load maximum at 3.4 MV.

2. *Thermal studies and quench location*

The section of the HOM filter emerging out of the DQW cavity is equipped with its own helium jacket. A cooling channel is opened in the main filter body for passive cooling of the hottest region, the tip of the hook [25]. The heat flux in 2 K superfluid helium is about 1 W/cm^2. The cooling channel of the HOM filter, with a section of 1 cm^2, is sized to extract about 1 W of heat.

In the LHC configuration, cavity and filter will be surrounded by a limited helium volume given by the space between the helium jacket and the niobium walls of the HOM filter. However, for these tests, the cavity was without its helium jacket and the top cap of the filter's helium jacket was not assembled to allow the installation of a couple of thermosensors by the cooling channel aperture (see Fig. 37). The thermosensors registered a temperature increase on this location for several tests (Test II in May'17, Test V in Oct'17, and Test IX in Sep'18), which suggested a thermal runaway initiating in some part of the main filter body.

The thermal behaviour of the HOM filter was studied for different voltage levels with CST [26]. The study considers the temperature dependence of the thermal conductivity and the BCS surface resistance for niobium [27] (BCS surface resistance for niobium at 2 K is 1 nΩ), and assumes a residual surface resistance of 5 nΩ. For operation at 4.1 MV, the temperature in the surroundings of the cooling channel is still 2 K, as shown in Fig 38. The maximum temperature is found in the tip of the hook. Above 4.5 MV, the power dissipated in the hook gets larger than 1 W (see Fig. 39) and the filter becomes thermally unstable, what probably causes the quench at 4.7 MV observed in the Test VII (May'18).

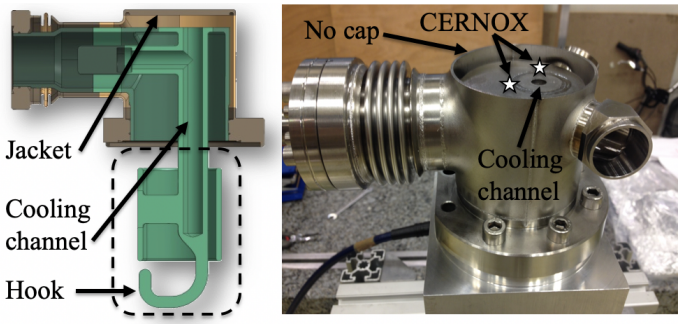

FIG. 37: [Left] Section view of HOM filter; the region receiving BCP is framed. [Right] Detail of the jacketed HOM filter used for cold tests without the top cap.

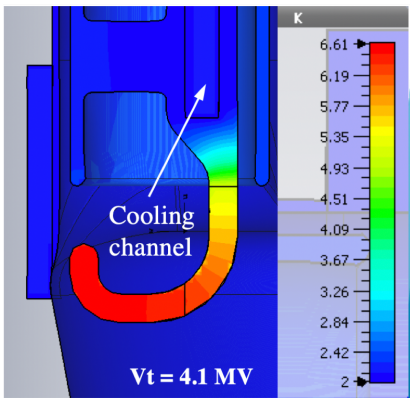

FIG. 38: Temperature distribution in the HOM filter for deflecting voltage of 4.1 MV.

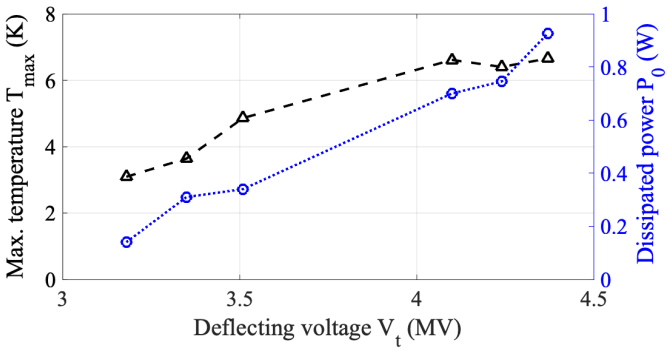

FIG. 39: Maximum temperature and power dissipated in HOM filter in function of the deflecting voltage.

3. *Effect of retracting the HOM filter*

To discriminate if the quench was originated from the cavity or the filter, a 20 mm-thick NbTi spacer was inserted between the HOM filter and its cavity port. If previous tests were limited by the HOM filter, due to large peak fields or large dissipated heat, the retracted HOM filter could not possibly be the limitation, because retracting the HOM filter by 20 mm reduced the fields in the filter by a factor 2 and the dissipated heat in the hook by a factor 4.

Higher voltages were reached with this configuration – 5.1 MV, as demonstrated in the Test IX (Sep'18) – close to the values obtained in the bare test of the DQW2 cavity – 5.3 MV in Sep'17. The Q-switch of 1.7×10^{10} appearing in the Test IX (Sep'18) at 1.6 MV (see Fig. 36) is attributed to the NbTi spacer becoming normal conductor.

While the retraction of the filter allows reaching higher voltages, it is not considered a solution because it reduces the coupling to some modes and consequently the damping. The pursue of even higher voltages, if needed, will require a revision of the HOM filter thermal properties.

Fig. 40 displays $Q_0 - V_t$ curves and radiation dose rate for all the DQW2 cavity tests with and without filters.

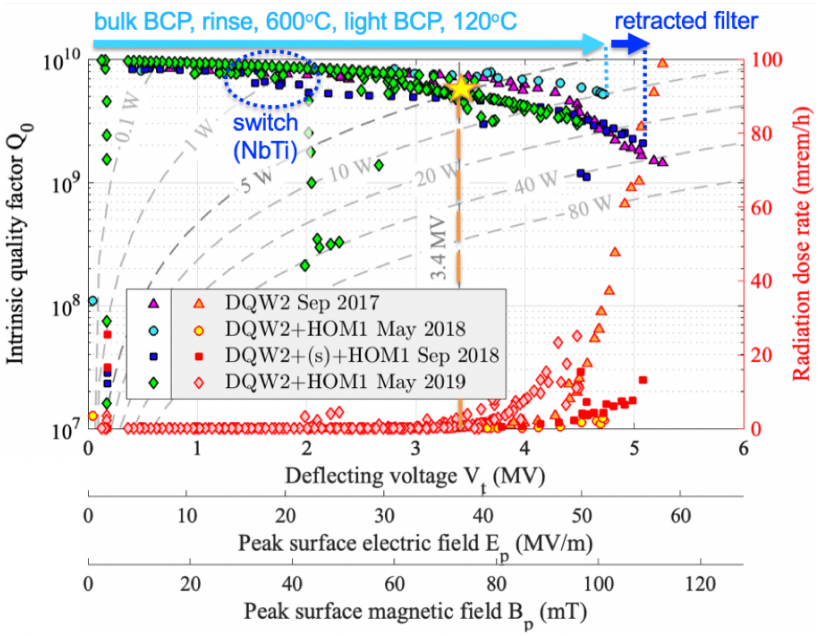

FIG. 40: Q_0 vs V_t curves for collection of DQW2 cavity tests, with and without HOM filter, illustrating the effect of HOM filter retraction on cavity performance.The yellow star marks the target of 5 W heat load maximum at 3.4 MV.

C. Lorentz Force Detuning

The cold test frame, shown in Fig. 9, does not fully reproduce the boundary conditions of a DQW cavity in the cryomodule. The expected LFD for a jacketed DQW cavity is about -40 Hz/(MV^2). Measured LFD during cold tests is about -(500–600) Hz/(MV^2). After removing the rods fixing the capacitive plates to the stiffening frame for test on Jan'18, the LFD increased to about -(700–800) Hz/(MV^2). This was expected because the capacitive plates, in the high electric field region, were let free, and so the Lorentz force would attract them together, increasing their capacitance and thus reducing the cavity frequency.

D. Multipacting Bands

Table IX summarizes the multipacting bands predicted by simulations for the DQW SPS-series cavity and the multipacting bands found during the tests. Fig. 41 shows the different cavity regions where multipacting sites are predicted and their impact energy and band. The multipacting predictions by ACE3P and CST matched well the multipacting bands found during the tests. A recurrent multipacting band, below 0.5 MV, related to multipacting in the cavity waist as predicted by ACE3P and CST, was found in every single test. Other multipacting bands processed and never came back in following tests.

Predicted by simulations			Found during tests without filter	
Band (MV)	Region	Code	Band (MV)	Description
0.26	Cavity waist	CST	0.17, 0.2	Hard. Conditioned 1.5 h at 10-20 W input power before first breach through. Every quench will cause cavity to drop into this zone for about 30 minutes. Found for every test.
0.1–0.5	Cavity waist	ACE3P		
1.06	Cavity-small port	CST	1.1	Soft
1.0–2.5	Waist	CST	1.9, 2.3	Soft
0.8–3.5	Dome	CST	1.9, 2.3, 3.0	Soft
1.6–3.0	Cavity-beam port, cavity-small port	ACE3P	1.9, 2.3, 3.0	Soft
4.0–4.5	Dome	ACE3P	4.5	Soft. Quenched into this band for a few minutes.
Predicted by simulations			Found during tests with or w/o filter	
Band (MV)	Region	Code	Band (MV)	Comments
0.26	Cavity waist	CST	0.17, 0.2	Hard. Conditioned 1.5h at 10-20 W input power before first breach through. Every quench will cause cavity to drop into this zone for about 30 minutes. Found for every test.
0.1–0.5	Cavity waist	ACE3P		
2.12	HOM stub	CST	1.8–2.3	Soft
			2–3	Soft

TABLE IX: Comparison between multipacting bands predicted by simulations and those found during cold tests

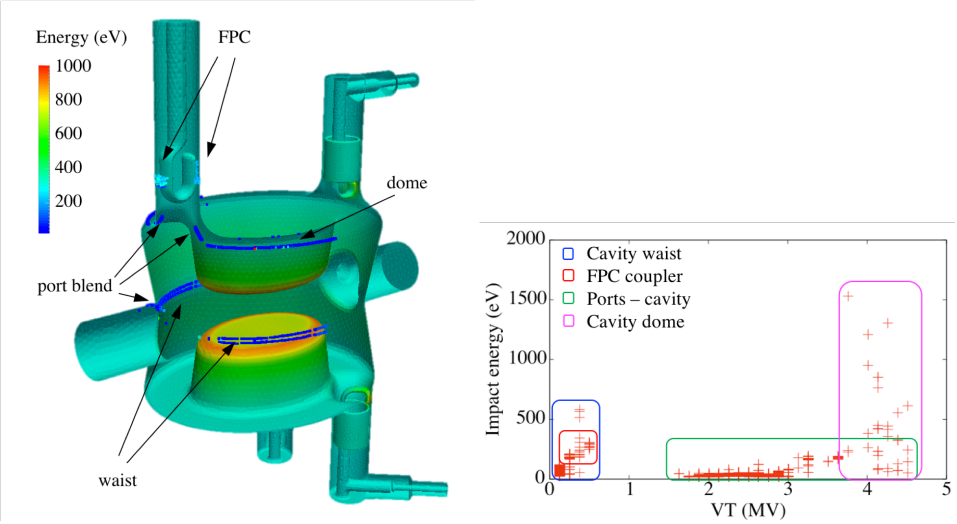

FIG. 41: [Left] Cavity regions where multipacting sites are predicted by ACE3P and [right] their impact energy and band [6].

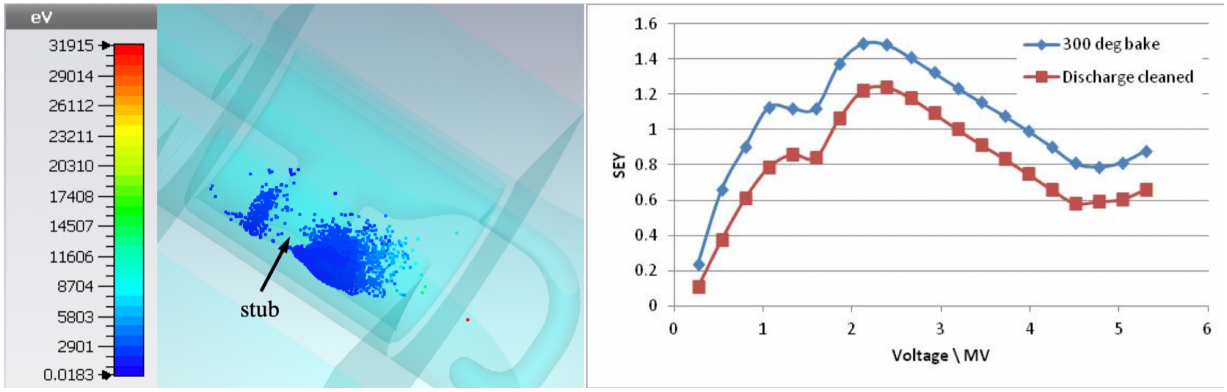

FIG. 42: [Left] HOM filter region where multipacting sites are predicted by CST and their impact energy; [right] secondary emission yield (SEY) and band for multipacting sites in HOM filter [28].

E. Field-Emission Onset and Quench Voltages

The tests with 2 HOM filters found some early field-emission onset at 1.5 – 2.4 MV. However, tests with only 1 HOM filter are encouraging: field emission can appear as late as for bare cavity tests. There were 3 successful tests for a bare cavity with 1 HOM fields that reached a deflecting voltage above 4.5 MV with a field-emission onset above 2.8 MV, not so far from the nominal deflecting voltage. Fig. 43 summarizes the field-emission onset and quench voltages found for the LARP DQW SPS-series cavities.

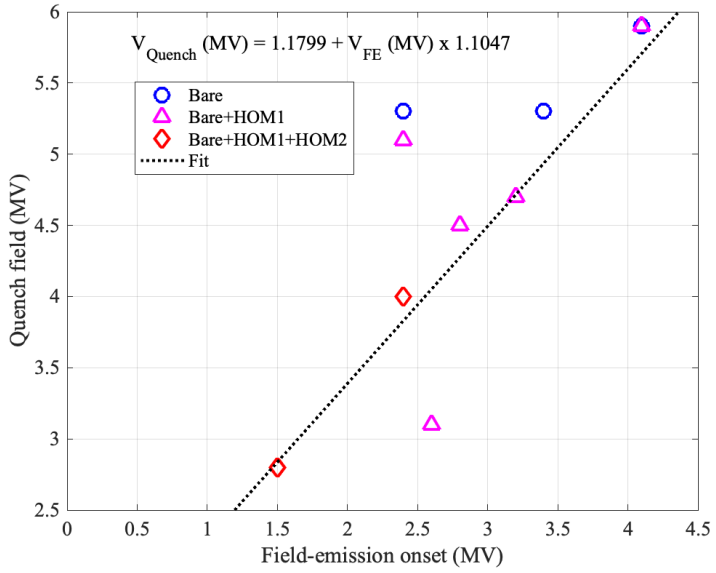

FIG. 43: Field-emission onset and quench voltages for cold tests of the LARP DQW SPS-series cavities.

F. Coupling Evolution for Test Probes

Table X lists the evolution of the coupling for the two probes (input and pickup probes) used for the cryogenic RF tests.

Assembly	Test	External Q for input probe (Q_1)	External Q for pickup probe (Q_2)
Design	CST	2e9	8e11
DQW01	Warm	1.92e9	1.77e12
	Test I (Feb'17)	2.07e9	1.60e12
DQW02	Warm	1.83e9	1.19e12
	Test III (Jun'17)	2.05e9	1.78e12
	Test IV (Sep'17)	1.83e9	1.20e12c
DQW01+HOM01	Test II (May'17)	2.10e9	1.47e12
DQW02+HOM01	Test V (Oct'17)	1.93e9	1.21e12
	Test VI (Jan'18)	2.15e9	1.27e12
	Test VII (May'18)	2.12e9	1.21e12
	Test VIII (Jul'18)	1.93e9	1.15e11
	Warm	n/a	6.28e12
	Test IX (Sep'18)	2.08e9	2.74e12
	Test X (May'19)	1.84e9	1.24e12
DQW02+HOM01+HOM02	Test XI (Jul'19)	1.9e9	3.4e13
	Warm	1.8e9	2.2e12
	Test XII (Oct'19)	1.8e9	2.2e12

TABLE X: Coupling evolution for test probes

V. CONCLUSIONS & OVERVIEW

The availability of prototypes proved useful to investigate the performance limitations and define surface treatment procedures for the HL-LHC DQW cavities. The CERN DQW SPS-series were installed by mid 2017 into their cryomodule for beam tests in SPS. At the time, the performances of the four DQW SPS-series prototypes was in the range of 4.7 – 5.9 MV [6, 16, 29] for bare cavity cold tests, well above the 3.4 MV nominal deflecting voltage and reaching magnetic field values as high as 125 mT (B_p/V_t = 21.2 mT/MV), but the performances of a DQW SPS-series cavity with HOM filters did not exceed 3.3 MV. Thanks to this test campaign, we could find the pathway to operate dressed crab cavities at higher voltages beyond required levels.

The excellent results found during this test campaign highlight the maturity of the design of the DQW cavity and its HOM filters and shed light on the necessary preparations to ensure that the HL-LHC requirements are fulfilled.

These are the lessons learned during this test campaign:

- The HOM filters should receive the same surface treatment as any other SRF cavity.
- A standard SRF surface treatment (bulk BCP, high-temperature degassing, light BCP, low-temperature bake) for cavity and filter is sufficient to exceed the required deflecting voltage (4.7 MV before quench) with a comfortable margin (38%). The cryogenic load is lower than 10 W at 4.1 MV with pretty low surface resistance of 10 nΩ at low fields.
- Large peak fields can be reached with a DQW cavity equipped with its HOM filters – 106 mT in cavity at quench field of 4.7 MV – but still not as high as for other niobium cavities that followed a BCP-based surface treatment, like the bare DQW SPS-series cavities. A quench in the HOM filter, likely of thermal nature, limits Continuous-Wave (CW) operation.
- Demonstrated successful manufacture by industry of DQW cavities.

The DQW SPS-series cavities and their HOM filters find two main operational limitations that are not critical:

- Earlier quench field for dressed cavity than for bare cavity, likely caused by insufficient cooling in the HOM filter. This earlier quench field reduces the advantageous margin presented by the bare DQW SPS-series cavity.
- Recurring multipacting band below 0.5 W is difficult to make disappear. The beam tests of the DQW cryomodule in SPS did not find, however, major operational complications related to the presence of this multipacting band.

Some improvements towards the HL-LHC-series production were identified:

- Make the length of the short beam port as long as the longest beam port to reduce heat load in the joint.
- Enlarge the cooling channel if possible to provide more cooling capacity and therefore increase the margin over the operational deflecting voltage required for the HL-LHC crab cavities.
- Another improvement came from the lessons learned during the beam tests of a fully equipped DQW cryomodule in the SPS. The pickup antenna showed some direct coupling to the beam. The antenna design was changed to reduce the direct coupling. Another small port was opened on one of the beam ports to host a dedicated antenna for extraction of the 1.754 GHz HOM power.
- Apply a full surface treatment to the HOM filters.
- Modify the test probes, made in copper, to include a stainless-steel threaded hole insert. The current test probes had the threaded hole made in copper. After several uses, the thread was damaged and compromised the correct fixing of the probe to the feedthrough.

The DQW LHC-design characteristics are summarized in Table II. Modifications exclusively affect some cavity ports and RF ancillaries [11]. None of the improvements implies a change of the main body of the DQW cavity, where the maximum peak fields are located. Thus, performance beyond the nominal with extraordinary margin can be also expected for LHC-series. In the near future, the LARP DQW SPS-series cavities will be used to test the effects of electropolishing by KEK.

ACKNOWLEDGMENTS

We are grateful to Niowave Inc. for lending us the cavities used for these tests and to the JLab SRF facility team for their support during the tests of the cavities.

[1] R. Calaga, E. Jensen, G. Burt, and A. Ratti, “Crab cavity development”, in The high luminosity large hadron collider, O. Brüning and L. Rossi, Ed. Geneva,Switzerland: World Scientific, 2015, vol. 22, pp. 137 – 156. doi:10.1142/9581

[2] L. Alberty et al., “Engineering specification: Dressed bulk niobium radio-frequency crab cavities", LHC-ACFDC-ES-0002, EDMS No. 1389669 (2019).

[3] R. Calaga, S. Belomestnykh, I. Ben-Zvi, J. Skaritka, Q. Wu, and B. P. Xiao,“A double quarter wave deflecting cavity for the LHC”, in *Proc. IPAC’13*, Shanghai, China, May 2013, paper WEPWO047, pp. 2408 – 2410.

[4] I. Ben-Zvi, “The quarter-wave resonator as a crab cavity", presented at the 4th LHC Crab Cavity Workshop, CERN, Geneva, Switzerland, Dec. 2010, unpublished.

[5] B. P. Xiao *et al.*, “Design, prototyping and testing of a compact superconducting double quarter wave cavity”, *Phys. Rev. ST Accel. Beams*, vol. 18, p. 041004, 2015. doi:10.1103/PhysRevSTAB.18.041004

[6] S. Verdú-Andrés *et al.*, “Design and vertical tests of double-quarter wave cavity prototypes for the high luminosity LHC crab cavity system”, *Phys. Rev. ST Acc. Beams*, vol. 21, p. 082002, 2018. doi:10.1103/PhysRevAccelBeams.21.082002

[7] B. P. Xiao *et al.*, “Higher order mode filter design for double quarter wave crab cavity for the LHC high luminosity upgrade”, in *Proc. IPAC’15*, Richmond, VA, USA, May 2015, pp. 3627–3629. doi:10.18429/JACoW-IPAC2015-WEPWI059

[8] J. A. Mitchell *et al.*, “DQW HOM coupler design for the HL-LHC", in *Proc. of the 9th International Particle Accelerator Conference (IPAC’18)*, Vancouver, BC, Canada, May 2018, paper THPAL018, pp. 3663 - 3666.

[9] J. A. Mitchell, “HOM damping and SPS measurements", presented at the International Review of the Crab Cavity System Design and Production Plan for the HL-LHC, CERN, Geneva, Switzerland, Jun. 2019, unpublished.

[10] J. A. Mitchell, PhD Thesis, University of Lancaster, Aug. 2019, to be published.

[11] S. Verdú-Andrés *et al.*, “Design of LHC Crab Cavities Based on DQW Cryomodule Test Experience”, in *Proc. SRF’19*, Dresden, Germany, Jun.-Jul. 2019.

[12] B. P. Xiao, “Using pickup coupler for 1.75 GHz HOM", Jun. 2015, unpublished.

[13] EDMS No. 1400295 - Drawing LHCACFCA0001: https://edms.cern.ch/document/1400295/AE

[14] R. Calaga, O. Capatina, and G. Vandoni, “The SPS tests of the HL-LHC crab cavities”, in *Proc. IPAC’18*, Vancouver, BC, Canada, Apr.-May 2018, pp. 846 – 849. doi:10.18429/JACoW-IPAC2018-TUPAF057

[15] EDMS No. 1494836 - Drawing LHCACFHC0001: https://edms.cern.ch/document/1494836/1

[16] S. Verdú-Andrés *et al.*, “Cryogenic RF performance of double-quarter wave cavities equipped with HOM filters", in *Proc. of the 10th International Particle Accelerator Conference (IPAC’19)*, Melbourne, Australia, USA, May 2019, paper WEPRB098.

[17] S. Verdú-Andrés *et al.*, *Thermal losses in couplers and ports of a SPS Double-Quarter Wave crab cavity*, in Proc. of SRF‘15, THPB052, Whistler, Canada (2015).

[18] A. Hernández, E. Martín, J. Margineda and J. M. Zamarro, “Resonant cavities for measuring the surface resistance of metals at X-band frequencies", J. Phys. E: Sci. Instrum. **19** (1986).

[19] N. Shipman, “DQW coupler summary", Dec. 2016, unpublished.

[20] B. P. Xiao and T. Xin, “Report on activities at JLab for Double Quarter Wave Crab Cavities", Jan. 2017, unpublished.

[21] B. P. Xiao, "Double Quarter Wave Crab Cavity Cryogenic Test with HOM Filter", Oct. 2017, unpublished.

[22] Q. Wu, “BNL visit to Jlab for SPS DQW prototypes processing", Dec. 2016, unpublished.

[23] B. P. Xiao, "NW-LARP-DQW#2 Cavity + HOM Coupler Cold Test Report", Oct. 2017, unpublished.

[24] B. Aune, R. Bandelmann, D. Bloess, B. Bonin, A. Bosotti, M. Champion, C. Crawford, G. Deppe, B. Dwersteg, D. A. Edwards, H. T. Edwards, M. Ferrario, M. Fouaidy, P.-D. Gall, A. Gamp, A. Gössel, J. Graber, D. Hubert, M. Hüning, M. Juillard, T. Junquera, H. Kaiser, G. Kreps, M. Kuchnir, R. Lange, M. Leenen, M. Liepe, L. Lilje, A. Matheisen, W.-D. Möller, A. Mosnier, H. Padamsee, C. Pagani, M. Pekeler, H.-B. Peters, O. Peters, D. Proch, K. Rehlich, D. Reschke, H. Safa, T. Schilcher, P. Schmüser, J. Sekutowicz, S. Simrock, W. Singer, M. Tigner, D. Trines, K. Twarowski, G. Weichert, J. Weisend, J. Wojtkiewicz, S. Wolff, and K. Zapfe, Superconducting TESLA cavities, Phys. Rev. ST Accel. Beams **3** 092001 (2000).

[25] F. Carra *et al.*, “Assessment of thermal loads in the CERN SPS crab cavities cryomodule”, *J. Phys.: Conf. Ser.*, vol. 874, p. 012005, 2018. doi:10.1088/1742-6596/874/1/012005

[26] CST Studio Suite, version 2018, Computer Simulation Technology Program, CST AG, Darmstadt, Germany.

[27] P. Dhakal *et al.*, “Superconducting DC and RF properties of ingot niobium", in *Proc. SRF’11*, Chicago, IL, USA, Jul. 2011, paper THPO057, pp. 856 – 861.

[28] G. Burt, priv. comm., Mar. 2018.

[29] A. Castilla, “CERN DQW cavity results”, presented at HiLumi’17, Ciemat, Madrid, Spain, Oct. 2017, unpublished. https://indico.cern.ch/event/647714/contributions/2651553/attachments/1557480/2496073/cern_dqw_sum_v10.pdf